The determination of an accurate isotope dependent potential energy surface for water from extensive *ab initio* calculations and experimental data

Harry Partridge and David W. Schwenke
NASA Ames Research Center, Moffett Field, California 94035-1000

(Received 13 November 1996; accepted 9 December 1996)

We report on the determination of a high quality *ab initio* potential energy surface (PES) and dipole moment function for water. This PES is empirically adjusted to improve the agreement between the computed line positions and those from the HITRAN 92 data base with $J \leqslant 5$ for $H_2{}^{16}O$. The changes in the PES are small, nonetheless including an estimate of core (oxygen 1*s*) electron correlation greatly improves the agreement with the experiment. Using this adjusted PES, we can match 30 092 of the 30 117 transitions in the HITRAN 96 data base for $H_2{}^{16}O$ with theoretical lines. The 10, 25, 50, 75, and 90 percentiles of the difference between the calculated and tabulated line positions are -0.11, -0.04, -0.01, 0.02, and 0.07 cm^{-1}. Nonadiabatic effects are not explicitly included. About 3% of the tabulated line positions appear to be incorrect. Similar agreement using this adjusted PES is obtained for the ^{17}O and ^{18}O isotopes. For $HD^{16}O$, the agreement is not as good, with a root-mean-square error of 0.25 cm^{-1} for lines with $J \leqslant 5$. This error is reduced to 0.02 cm^{-1} by including a small asymmetric correction to the PES, which is parameterized by simultaneously fitting to $HD^{16}O$ and $D_2{}^{16}O$ data. Scaling this correction by mass factors yields good results for T_2O and HTO. The intensities summed over vibrational bands are usually in good agreement between the calculations and the tabulated results, but individual line strengths can differ greatly. A high-temperature list consisting of 307 721 352 lines is generated for $H_2{}^{16}O$ using our PES and dipole moment function. © *1997 American Institute of Physics.*
[S0021-9606(97)03810-5]

I. INTRODUCTION

The rovibrational spectrum for the ground state of water is of considerable interest for a number of applications. These areas include astronomy and astrophysics, studies involving the atmospheres of planets, and simulations involving combustion. Consequently, there is a large amount of experimental data. The consumers of the water spectra require line positions and line intensities at particular temperatures over a wide range of intensities. In principle, much of this information can be obtained from experiment, but in practice this is difficult because it is necessary to properly assign all of the transitions in order to model the temperature dependence. Also, weak transitions are difficult to measure under terrestrial conditions. For astrophysical applications in particular, the existing data bases are inadequate. On our sun, there are about 50 lines/cm^{-1} in the sunspot spectrum,[1] and experimental data bases only allow the assignment of a handful of lines to water, even though many more water lines are present. In cooler stars with surface temperatures in the range 2000–4000 K, there can be a high concentration of molecular species in their atmospheres. Consequently, the spectra of these stars are very complex, being dominated by many overlapping molecular bands containing typically 10^4-10^7 lines each. For oxygen rich stars, water can be a major absorber,[2] and the large number of very weak lines can be an important factor governing the predicted size of the stellar atmospheres.[3] In contrast to the experimental situation, theoretical calculations of the opacity are more straightforward in that a complete and consistent data set can be generated. The challenge is to obtain sufficient accuracy in the data. Theoretical spectra have been generated for astrophysical applications, but the existing spectra[4–6] are not sufficiently complete and accurate. In the present work we present results that are of much higher accuracy and completeness than previously reported.

Significant progress has been made in algorithms for computing the rotational–vibrational energy levels and intensities of triatomic molecules. Thus, this aspect of the problem is largely solved. The calculations require both an accurate potential energy surface (PES) and a dipole moment surface (DMS). *Ab initio* calculations provide an efficient method for determining the DMS. However, very high quality is required for the PES because it is necessary to predict the rotational–vibrational energy levels to very high accuracy, to better than 0.1 cm^{-1}. While the accuracy of *ab initio* calculations has improved dramatically in recent years,[7] the errors in the best polyatomic potential energy surfaces are still two to three orders of magnitude larger than this. Benchmark calculations have shown that the convergence with basis set expansion is slow. In addition, effects often neglected, such as core correlation (oxygen 1*s*) shifts the harmonic frequencies significantly.[8] Hence, while the errors in the computed potential energy surfaces should be systematic, it will be necessary to use experimental data to refine any *ab initio* potential in order to achieve spectroscopic accuracy. Currently the best available PESs[9–11] for $H_2{}^{16}O$ are based on optimization of model potential parameters via a least squares fit to measured rotational–vibrational levels with essentially no input from *ab initio* calculations. In contrast, by starting from the *ab initio* potential and then making small

 0021-9606/97/106(11)/4618/22/$10.00

corrections to it, we can obtain higher accuracy with fewer parameters. It appears that this is possible only when the *ab initio* potential is of sufficiently high quality. In addition to fitting the existing experimental data better than a completely empirical PES, it is expected that our PES will give a much more reliable extrapolation to regions not sampled by low temperature experimental data.

In this work we report *ab initio* calculations for water that are significantly more accurate and extensive than previous work.[4,12–16] We will present a fit to the *ab initio* energies and dipole moment. We optimize selected parameters in the fit of the PES to improve the agreement with the observed rovibrational transitions. We show that the differences in the parameters from the *ab initio* fit are small and the changes in the PES are consistent with the changes expected with improvements in the calculations. This PES and DMS are used to generate a high-temperature (4000 K) line list for water.

The rovibrational energy levels are obtained from variational calculations using an exact kinetic energy operator and analytic basis functions and do not explicitly include nonadiabatic corrections. The experimental data used for adjusting the PES is taken primarily from the HITRAN 92 data base.[17] However, comparisons are also made to the HITRAN 96 data base,[18] which became available during the course of this work.

This paper is organized as follows: in Sec. II we discuss our *ab initio* methods, in Sec. III we give the fit to the PES, followed by the fit to the DMS in Sec. IV. In Sec. V we give our methods for determining the rovibrational energy levels. This is followed by the description of the empirical modifications to the PES in Sec. VI, a discussion of the results obtained on that PES in Sec. VII, our results for the different isotopes in Sec. VIII, and then a comparison of the empirical PES and the expected errors in the *ab initio* results in Sec. IX. Finally, we give our conclusions in Sec. X.

II. *AB INITIO* METHODS

The basis sets employed are the correlation consistent polarized valence basis sets of Dunning and co-workers.[19] These basis sets have been optimized to obtain the atomic correlation energy. The incremental energy lowerings were found to fall into distinct groups,[19] providing a criteria for obtaining systematic convergence to the complete basis set limit. The PES that is reported utilizes the cc-pV5Z basis set augmented with a diffuse s, p, and d on oxygen and an s and p on hydrogen. The exponents for the diffuse functions are taken from the augmented (aug) correlation consistent sets. The oxygen basis set is of the form $(15s\ 9p\ 5d\ 3f\ 2g\ 1h)/[7s\ 6p\ 5d\ 3f\ 2g\ 1h]$ and the hydrogen basis is of the form $(9s\ 5p\ 3d\ 2f\ 1g)/[6s\ 5p\ 3d\ 2f\ 1g]$. Calibration calculations utilize the cc-pVTZ, cc-pVQZ, and the cc-pV6Z[20] basis sets. The cc-pVTZ and cc-pVQZ sets are augmented in the same manner as the cc-pV5Z set using the corresponding augmented set. The cc-pV6Z basis set is not augmented because of the computational expense and previous work[21] on N_2 indicates that additional augmentation is unnecessary. In short, we will call these basis sets TZ, QZ, 5Z, or 6Z. The number of contracted functions in the calculations were TZ(75), QZ(132), 5Z(218), and 6Z(322).

To study the effect of the $1s$ correlation, the cc-pVQZ set is modified. The seven inner $1s$ functions are contracted to two functions using the coefficients from the cc-pVQZ basis set. The outer five s functions are uncontracted as are the six p functions. Two tight d and f functions are added to the $(3d\ 2f\ 1g)$ polarization set given by Dunning. The exponents of the added functions are 10.962 and 31.83 for the d functions and 8.274 and 25.68 for the f functions. The basis set is augmented with a diffuse s, p, and d on oxygen and an s and p on hydrogen using the aug-cc-pVQZ exponents. This core basis set, developed to treat both core and valence correlation, is of the form $(12s\ 6p\ 5d\ 4f\ 1g)/[7s\ 6p\ 5d\ 4f\ 1g]$, and is designated CQZ. For calibration, a cc-pV5Z core set (C5Z) is derived in a similar manner. The outer six s functions are uncontracted as are the eight p functions. The basis set is augmented with the diffuse functions used for the valence basis set and with two tight d, f, and g polarization functions; the exponents are d (14.7, 36.74), f (10.04, 25.1), and g (8.38, 20.94).

The orbitals are optimized using the complete active space self-consistent-field (CASSCF) approach. All of the calculations are performed in C_s symmetry with six a' and two a'' orbitals and eight electrons active. This active space gives a balanced description for all geometries. More extensive correlation is included using the multireference configuration-interaction (MRCI) approach. All configurations in the CASSCF wave function are used as references in the MRCI calculations. The same reference space is used when the $1s$ correlation is treated. The effect of higher excitations is accounted for using the multireference analog of the Davidson correction (denoted +Q). The internal contraction[22] (IC) is utilized to keep the calculations manageable. The dipole moment was calculated as an expectation value.

In Table I we investigate the convergence with respect to the level of correlation in the TZ-based basis set. The difference between the ICMRCI+Q and MRCI+Q results shows that the internal contraction error is small, but increases with the excitation energy. Expanding the active space has only a small effect on the ICMRCI+Q results. Previous comparisons[23] have shown that the ICMRCI and MRCI results converge as the active space is expanded. This suggests there is a cancellation of errors, as the difference between the ICMRCI+Q results is small for the (62) and (84) active spaces. These calculations suggest that the error introduced by evaluating the dipole moment as an expectation value rather than an energy derivative is small. Note, however, that the dipole moment calculated in this way does not include the effect of the Davidson correction.

In Table II we report the core correlation contribution determined at various levels of theory. The correction ΔV^{core} is defined as the difference of the energies from a valence only and core and valence electron calculation. For these calculations, we use the averaged coupled pair func-

TABLE I. Convergence of potential with correlation treatment. The zero of energy is at $r_1=r_2=0.9587$, $\theta=104.3850$. Bond lengths in Å, angle in degrees, and energies in cm^{-1}.

Geometry			ICMRCI+Q	MRCI+Q		ICMRCI+Q	ICMRCI+Q	ICMRCI+Q
θ	r_1	r_2	(6,2)[a]	(6,2)[a]	CCSD(T)	(7,3)[a]	(8,4)[a]	(9,4)[a]
160	0.9	1.0	10 804.62	10 826.05	10 786.38	10 805.79	10 801.38	10 803.86
170	0.9	1.0	12 251.49		12 232.38	12 255.85		
180	0.9	1.0	12 770.96		12 751.59	12 770.26		
140	0.9	1.0	6383.97		6370.16	6380.11		
120	0.9	1.0	2406.71	2415.21	2399.63	2403.65	2407.77	
100	0.9	1.0	1328.26		1327.45	1329.79		
80	0.9	1.0	4913.93	4904.25	4917.86	4920.47	4912.12	4911.92
60	0.9	1.0	14 769.42	14 748.22	14 774.16	14 799.00		
50	0.9	1.0	23 204.09	23 175.62	23 208.63	23 214.09		
40	0.9	1.0	36 553.09		36 560.36	36 558.54		

[a]The pair specifies the number of active orbitals in each symmetry.

tional (ACPF) method[24] or the coupled–cluster singles and doubles (CCSD) approach[25] including a perturbational estimate of the triple excitations[26] [CCSD(T)]. This is because it is necessary to use a size extensive method when different numbers of electrons are correlated.[21,27] Employing the CCSD(T) method to determine ΔV^{core} gives a core contribution that is slightly smaller than the ACPF results. This is consistent with previous results for other systems where the ACPF core contribution is larger than the CCSD(T) result. ΔV^{core} is insensitive to improvements in the basis set: the

TABLE II. Core contribution. Core contribution computed as energy difference E(valence)−E(core). CCSD(T) energy values reported to give indication of relative energies. The zero of energy is at $r_1=r_2=0.9587$, $\theta=104.3850$. Bond lengths in Å, angle in degrees, and energies in cm^{-1}.

Geometry			CCSD(T)	Core(CCSD(T))	Core(ICACPF)	Core(CCSD(T))
θ	r_1	r_2	CQZ	CQZ	CQZ	C5Z
60.00	0.80	0.90	26 391.79	68.175	69.883	
80.00	0.80	0.90	14 110.82	78.638	81.515	
100.00	0.80	0.90	9080.65	92.059	96.277	
104.52	0.80	0.90	8721.73	95.851	100.350	97.188
110.00	0.80	0.90	8610.83	100.860	105.673	
120.00	0.80	0.90	9198.06	111.120	116.409	
140.00	0.80	0.90	12 427.97	134.955	140.685	
160.00	0.80	0.90	16 190.11	157.515	163.089	
160.00	0.80	0.80	22 080.52	202.353	209.172	
170.00	0.80	0.80	23 210.10	208.685	215.965	
140.00	0.80	0.80	18 623.71	181.955	189.418	184.694
104.52	0.90	1.00	1185.30	9.418	9.925	
90.00	0.90	1.00	2433.54	−1.953	−2.792	
70.00	0.90	1.00	8914.86	−13.234	−15.866	
110.00	0.90	1.00	1339.51	14.595	15.576	
170.00	0.90	1.10	16 071.70	63.110	63.643	
160.00	0.90	1.10	14 501.91	52.836	53.842	53.675
140.00	0.90	1.10	9771.17	24.539	25.874	
120.00	0.90	1.10	5490.24	−1.517	−1.244	−1.481
110.00	0.90	1.10	4290.82	−12.045	−12.622	
104.52	0.90	1.10	4014.93	−17.073	−18.157	
100.00	0.90	1.10	4018.60	−20.841	−22.356	−21.086
60.00	0.90	0.95	15 468.74	−1.870	−4.150	
80.00	0.90	0.95	4992.74	8.478	7.686	
100.00	0.90	0.95	1028.03	22.195	23.181	
104.52	0.90	0.95	851.66	26.109	27.478	
110.00	0.90	0.95	940.98	31.299	33.114	
120.00	0.90	0.95	1846.92	42.045	44.567	
140.00	0.90	0.95	5610.47	67.655	70.956	
160.00	0.90	0.95	9816.55	93.180	96.281	
170.00	0.90	0.95	11 185.57	101.716	104.571	
175.00	0.90	0.95	11 551.74	104.038	106.810	
180.00	0.90	0.95	11 676.04	104.830	114.226	

.

TABLE III. Convergence with basis set expansion. The zero of energy is at $r_1=r_2=0.9587$, $\theta=104.3850$. Bond lengths in Å, angle in degrees, and energies in cm^{-1}.

Geometry			Basis set				
θ	r_1	r_2	TZ	QZ	5Z	6Z	Extrapolated
180	0.9	1.0	12 770.11	12 635.18	12 572.19		12 517.0
170	0.9	1.0	12 250.68	12 121.27	12 061.22	12 030.69	11 999.1
160	0.9	1.0	10 803.90	10 689.61	10 637.12	10 611.47	10 587.0
140	0.9	1.0	6383.55	6307.45	6273.21		6245.2
120	0.9	1.0	2406.55	2355.52	2337.79	2331.72	2328.6
100	0.9	1.0	1328.17	1301.46	1302.07		
80	0.9	1.0	4913.60	4905.81	4914.04	4915.44	4915.7
60	0.9	1.0	14 768.43	14 753.11	14 751.53	14 749.67	
50	0.9	1.0	23 202.55	23 174.87	23 161.03	23 155.23	23 151.0
40	0.9	1.0	36 550.67	36 503.41	36 472.92		36 417.5

C5Z basis set gives nearly the same contribution as the CQZ basis set. This suggests that we are slightly overestimating the core contribution in this work.

In Table III we show the results of a basis set convergence study. The energies have not been corrected for basis set superposition error (BSSE). It is not clear how to correct for BSSE in the present situation. The basis set effect is largest for the near-linear points, which is expected based on symmetry arguments. If we assume that the energies converge logarithmically with improvement in the basis set, then we can extrapolate to the basis set limit,[28] and we include the extrapolated values in Table III. The extrapolations use the three largest basis sets given for each geometry. Note that extrapolation is not possible at all geometries—sometimes the energy oscillates. Other extrapolation formulas exist,[29] and using them as well gives some idea of the reliability of the extrapolations. This indicates an uncertainty of several cm^{-1}. It is interesting to compare the results of the two-point extrapolation formula[29] using the QZ and 5Z data to the results from the exponential extrapolation. The two-point formula gives the extrapolated energy as the 5Z energy plus 0.812 times the difference between the 5Z and QZ energies. Computing the average ratio of the difference between the extrapolated and 5Z energies to the difference between the 5Z and CQZ ACPF energies yields the fraction 0.87, which is close to the predicted value.

The ICMRCI and CCSD(T) calculations were performed with MOLPRO-94 (Ref. 30) and the uncontracted MRCI calculations were performed with MOLECULE/SWEDEN.[31] All calculations were carried out on a Cray C90 at the NASA Ames Research Center.

The geometries are specified by the two O–H bond lengths and the angle between them. The majority of the points computed correspond to a grid with $r=0.7$, 0.8, 0.9, 0.95, 1.0, 1.1, 1.2, 1.3, 1.5, and 1.7 Å and $\theta=30°$, 40°, 60°, 80°, 100°, 120°, 140°, 160°, 170°, and 180°. In addition, a number of points were added to characterize other regions of the surface. This includes points needed to determine a quartic representation, points describing $O+H_2$ and $OH+H$, and additional cuts within the grid.

The energy and dipole moment function were computed at 771 points using the 5Z basis set. For the points below 40 000 cm^{-1}, the core contribution was also determined using the CQZ basis. The geometries, energies, and dipole moments are available from E-PAPS.[32] The grid employed is sufficiently dense to accurately define the PES to 35 000–40 000 cm^{-1}. There are 285 points above 40 000 cm^{-1}, which are useful in helping define the high-energy portions of the surface, but the density of points is not sufficient to accurately specify the surface in this energy range. It should be noted that we have followed the lowest energy surface of A' symmetry. Thus, for the linear geometries we switch from the $^1\Sigma^+$ to the $^1\Pi$ states as r increases.

III. ANALYTIC REPRESENTATION OF THE PES

The most popular analytic representation of the PES for H_2O is the power series in the Morse transformed OH bond lengths and the cosine of the HOH angle that was introduced by Jensen.[33] In the present work we use an alternate form, more similar to the many body expansion popularized by Murrell and co-workers.[34] We do this for several reasons. The first is that the Jensen form is not capable of dissociating properly—even when only one bond length goes to infinity, the potential depends on the HOH angle. This is not to say that the present potential properly accounts for the complex crossings and avoided crossings in the asymptotic limits,[35] but it does become isotropic as any atom is pulled away. This improves the agreement with the *ab initio* energies of the H+OH geometries, which are given small weights in the fitting procedure. The second reason is that the representation of the potential for short HH distances is not reasonable. This can also be improved by adding a post-hoc correction term.[36] The final reason for preferring a different form is our difficulty in obtaining a globally reasonable fit using the Jensen expansion. In order to obtain small fitting errors, it was necessary to use a large number of terms, and the higher-order terms did not extrapolate very well, giving rise to spurious minima outside the region where data were present. Note the fit to the 5Z ICMRCI+Q energies used in Ref. 37 was a preliminary one using the Jensen expansion, and also included a fit to a preliminary estimate of the effects of core correlation.

The form finally adopted is

$$V^{5Z}(r_1,r_2,\theta)=V^a(r_1)+V^a(r_2)+V^b(r_{HH}) + V^c(r_1,r_2,\theta), \quad (1)$$

where the r_i are the OH bond lengths, θ is the HOH angle,

$$V^a(r)=D\{\exp[-2a(r-r_0)]-2\exp[-a(r-r_0)]\}, \quad (2)$$

$$V^b(r)=A\exp(-br), \quad (3)$$

r_{HH} the HH distance, and

$$V^c=c_{000}+\exp\{-\beta[(r_1-r_e)^2+(r_2-r_e)^2]\} \times\sum_{ijk} c_{ijk}[(r_1-r_e)/r_e]^i[(r_2-r_e)/r_e]^j \times[\cos(\theta)-\cos(\theta_e)]^k. \quad (4)$$

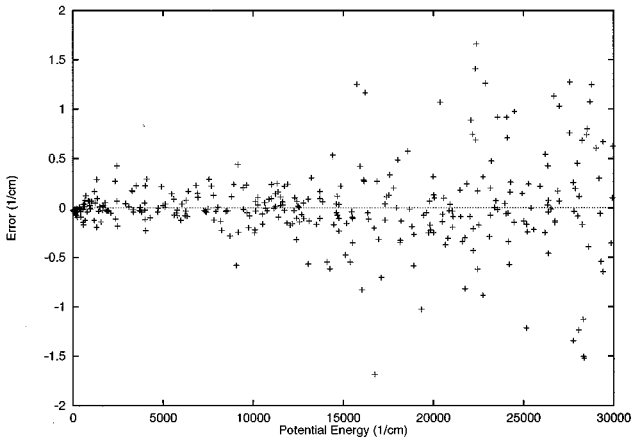

FIG. 1. Fitting errors of V^{5Z} as a function of the *ab initio* potential energy.

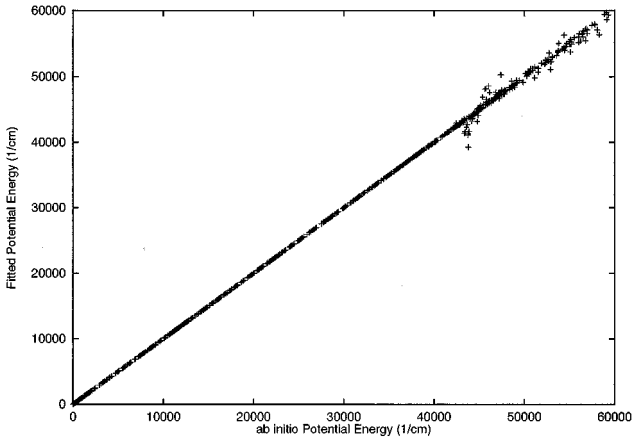

FIG. 2. The V^{5Z} energy as a function of the *ab initio* potential energy.

The parameters D, a, r_0, A, b, and the c_{ijk} were determined by performing an unequally weighted least squares fit to the *ab initio* data (ICMRCI+Q energies), the parameter β was fixed at $2a_o^{-2}$ to give fast enough damping (least squares optimization of this variable as well favored a much smaller value), and r_e and θ_e were fixed at preliminary estimates of the equilibrium geometry. The functions V^a and V^b are not meant to represent accurately the asymptotic OH and HH potential curves. Initial trials used a bound HH potential curve instead of V^b, but good results were not obtained.

An important question is how accurately we should attempt to fit the *ab initio* points. In principle one should fit them exactly, but this is not achievable in practice. A more pragmatic approach is to fit the energies to within their individual errors, which are fairly substantial although quite systematic. However, we have found it valuable to fit the points as well as possible and then empirically adjust the PES by matching experimental line positions; see Sec. VI below. We have found that better fits to the *ab initio* data give rise to better fits to the experiment when varying a given number of parameters. Thus, we ended up using in Eq. (4) $i+j \leqslant 8$, and $k \leqslant 14-(i+j)$ for a total of 245 c_{ijk}, after taking account of symmetry. A FORTRAN subprogram to evaluate this fit can be obtained from E-PAPS.[32]

Since the range of energies spanned by the *ab initio* calculations is large, it is necessary to unequally weight the points in the fitting procedure to obtain a satisfactory fit. The weighting scheme finally used was $w_i = s_i / E_i^w$ with

$$s_i = \{\tanh[-\alpha(V_i - V^{top})] + 1.002\,002\,002\}/2.002\,002\,002, \tag{5}$$

$$E_i^w = \max(10\,000\text{cm}^{-1}, V_i), \tag{6}$$

with $\alpha = 6\times10^{-4}$ cm, $V^{\text{top}} = 35\,000$ cm^{-1}, and V_i is the energy in cm^{-1} of point i above the minimum. The switch s_i goes from 1, for points with energies much below V^{top}, to 0.001, for points with energies much above V^{top}. The factor E_i^w is present to encourage the minimization of the relative error of the points, with a bias against low-energy points. This bias is included because the density of low-energy points is greater and the energies have finite precision. It would not be valuable to try to represent noise in the low-energy points at the expense of higher-energy points. Linear and near linear points where the electronic wave function changes character from $^1\Sigma$ to $^1\Pi$ were not included in the fit.

In Figs. 1–3 we show various aspects of the fit. In Fig. 1, we plot the fitting error versus the data for *ab initio* energies up to 30000 cm^{-1}, the highest energies where s_i is close to 1. The first point with an error greater than 1 cm^{-1} occurs at about 15 000 cm^{-1}, and the maximum error is less than 1.7 cm^{-1}. Of the 355 points in Fig. 1, 165 have errors less than 0.1 cm^{-1}. In Fig. 2, we plot the fitted versus the *ab initio* energies for *ab initio* energies up to 60 000 cm^{-1}. (There is one point with *ab initio* energy 59 873 cm^{-1} corresponding to O + H_2 which is off scale.) The fit behaves quite well up to these high energies. The points that deviate most are for H+OH geometries (nonbonded OH distance at least twice the equilibrium OH distance). These geometries have ener-

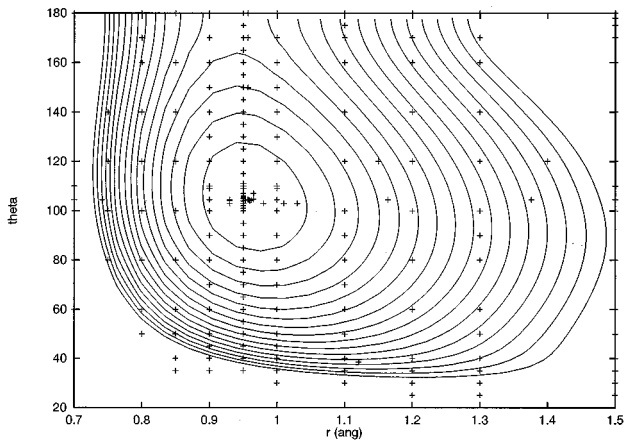

FIG. 3. Grid placement and contours for V^{5Z} for symmetric H_2O. The contour values are at increments of 2500 cm^{-1} and the symbols correspond to the *ab initio* points.

gies above 39 000 cm^{-1}. In Fig. 3, we show a contour plot of the fitted PES for symmetric geometries, along with points showing the *ab initio* grid. It would be hard to fit much higher in energy without additional points particularly at small r_i and small angle.

To include core correlation, we fit the difference in energies between the CQZ calculations with and without correlating the core (relative to their minimums). These calculations used the ACPF energies. This yields the correction $\Delta V^{\rm core}$, which is represented by Eq. (4) with $i+j+k \leqslant 6$, for a total of 50 c_{ijk}, after taking account of symmetry. The parameters can be obtained from E-PAPS.[32] A total of 371 points were included in the fit, and the points used the same weights as when fitting V^{5Z}. For V^{5Z} up to 30 000 cm^{-1}, the maximum error of the fit is 2.0 cm^{-1}, and this occurs at 28 523 cm^{-1}. The lowest energy with error greater than 1 cm^{-1} occurs at 23 108 cm^{-1}. Of the 336 points with energies below 30 000 cm^{-1}, 164 have errors less than 0.1 cm^{-1}.

As an estimate of the effect of a further basis set improvement, we also computed the difference between the CQZ valence and 5Z calculations. This gives the correction $\Delta V^{\rm basis}$, which is fit the same way as $\Delta V^{\rm core}$. The parameters can be obtained from E-PAPS.[32] For V^{5Z} up to 30 000 cm^{-1}, the maximum error of the fit is 1.6 cm^{-1}, and this occurs at 18 020 cm^{-1}. The lowest energy with error greater than 1 cm^{-1} occurs at 15 130 cm^{-1}. Of the 336 points with energies below 30 000 cm^{-1}, 160 have errors less than 0.2 cm^{-1}. Previous work has suggested that scaling $\Delta V^{\rm basis}$ is an effective procedure for including basis set corrections.[38]

On average, the magnitude of the core contribution is about twice the basis set correction. Both corrections have a geometry dependence and the shifts can be positive or negative. The basis set correction is largest for the linear points and lowers the relative energies. The core correction varies from -200 to 300 cm^{-1}. The magnitude is larger for the linear and small angle geometries and the magnitude increases as $r_{\rm OH}$ decreases.

IV. ANALYTIC REPRESENTATION OF THE DMS

To represent the DMS we follow the procedure of Ref. 39 and write

$$\boldsymbol{\mu}(r_1,r_2,\theta)=q(r_1,r_2,\theta)(\mathbf{x}_{\rm H_1}-\mathbf{x}_{\rm O}) + q(r_2,r_1,\theta)(\mathbf{x}_{\rm H_2}-\mathbf{x}_{\rm O}), \quad (7)$$

where q is a point charge and $\mathbf{x}_{\rm H_i}$, $\mathbf{x}_{\rm O}$ are position vectors of the atoms in a conveniently oriented coordinate system. The function q is a scalar and is independent of the definition of the body fixed coordinate axes. It can be expanded using the same type of functions as the potential, and the DMS will transform as a vector. Note that q is not symmetric with respect to interchanging r_1 and r_2. We use the dipole moment computed as an expectation value from the ICMRCI wave function using the 5Z basis.

We represent q by

$$q(r_1,r_2,\theta)=q^0(r_1,r_2,\theta)+q^c(r_1,r_2,\theta), \quad (8)$$

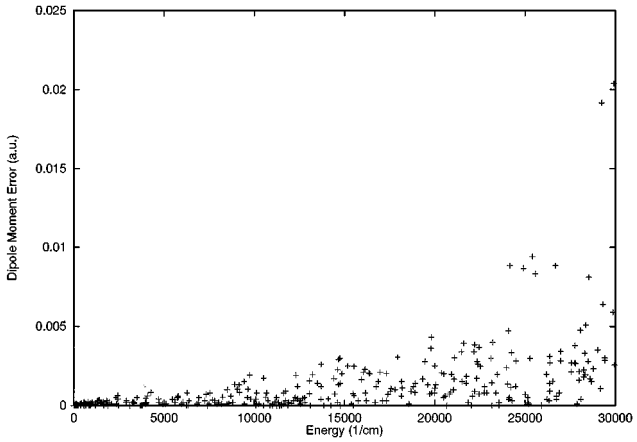

FIG. 4. Fitting errors of DMS as a function of the *ab initio* potential energy.

with q^0 a zero-order term and q^c a correction. We take

$$q^0(r_1,r_2,\theta)=A(r_1^{-b}+r_2^{-b}) \times[c_0+c_1P_1(\cos\theta)+c_2P_2(\cos\theta)], \quad (9)$$

where P_l is a Legendre polynomial, and q^c is given by the same expansion as used for V^c in Eq. (4). The parameters in q^0 were determined by approximately fitting the point charges determined by inverting Eq. (7) for symmetric geometries. The parameters in q^c were determined by a least squares fit using the functions with $i+j+k \leqslant 6$. A FORTRAN subprogram to evaluate the DMS is available from E-PAPS.[32] The same weights were used as in fitting the PES. In Fig. 4 we show the magnitude of the difference between the fitted and computed DMS for *ab initio* energies up to 30 000 cm^{-1}. The errors are usually quite small.

V. ROVIBRATIONAL CALCULATIONS

Transition intensities and energies were computed for a given PES and DMS using the procedures described in Ref. 39, with some improvements, which are described in the Appendix. Specific details are as follows. For $H_2{}^{16}O$, we used two different parameter sets. The first (set A) was used in the optimization of the PES, and was for $J \leqslant 5$. The second (set B) was used to generate a high-temperature line list, and used J up to 55. Where the parameter set differs in the discussion below, the values for set B are given in parentheses. The internal coordinates for symmetric isotopes were the Radau hyperspherical coordinates, and the llk coupling scheme was used for the angle. For asymmetric isotopes, Radau coordinates were used. Since, in the present work, a triatomic is involved whereas the development in Ref. 39 is for tetratomics, $l_3=0$ and $k=\Omega$ in the llk coupling scheme. The body frame z axis was aligned with one of the Radau vectors. Optimized stretching and rotation-bending basis functions were determined by performing a self-consistent-field (SCF) calculation on the lowest level for each JPS. The exact numerical parameters for stretches were chosen automatically,[40] using the criteria 10^{-5} for solving the one-dimensional Schrödinger equations with a cutoff of 0.3(0.35)

E_h and 10^{-6} for determining the optimized quadrature rules. For $J \geqslant 35$, this cutoff was reduced to $0.3E_h$, because the centrifugal potential was large enough to push the higher symmetric stretch levels into the continuum.

For $JPS=0++$, $H_2{}^{16}O$, this resulted in 23(30) contracted functions, 94(141) primitive functions, and an 18(23) point quadrature for the hyperradius, and 13(15) contracted functions, 30 primitive functions, and a 14/2 point quadrature for the hyperangle (symmetry allows us to use half of the quadrature points for the hyperangle). For the bend, we use associated Legendre functions P_{lm} with $l \leqslant 45$ and, when expanding the PES in terms of Legendre polynomials, we used 91 functions and a 91 point Gauss–Legendre quadrature. Contracted functions up to the energy cutoff of 0.17(0.24) E_h were determined. For $JPS=0++$, this resulted in 20(25) contracted functions. In the final coupling step, all functions with sums of SCF energies less than $0.3(0.35)E_h$ above the minimum energy were used, unless this number was greater than 5000(7500), in which case only the lowest 5000(7500) functions were used. (This happens for $J \geqslant 4$.) In the final diagonalization step, we explicitly exploit the symmetry decoupling due to the indistinguishability of the H atoms. This matrix was diagonalized using the routine DSYEV from LAPACK.[41] We determined all eigenvalues and eigenvectors in the energy range 0 to $0.1(0.15)$ E_h. Parameter sets similar in quality to set A were used for calculations for the other isotopes.

The dipole matrix elements required for the determination of the intensities were computed using the techniques described in Ref. 39. Specific numerical details are as follows: we expanded the angular dependence of the DMS using P_{lm} with $l \leqslant 26$ and used 28 point Gauss–Legendre quadrature to determine the expansion efficients and used a 20 point optimized quadrature for the hyperradius and a 15/2 point quadrature for the hyperangle. The use of a DMS that transforms as a vector obviates the need for special quadratures[42] over the angle.

All rovibrational calculations were carried out on an IBM RS-6000/590 work station equipped with 512 Mbyte of memory.

All calculations use the nuclear masses 1836.152 697, 3670.483 031, and 5496.921 62 m_e for the hydrogen isotopes and 29 148.946 42, 30 979.521 28, and 32 810.462 86 m_e for the oxygen isotopes, and used atomic units. To convert to cm^{-1} units, we divided by $4.556\,335 \times 10^{-6}$. To convert between Å and a_o, we used the factor 0.529 177 249.

VI. EMPIRICAL CORRECTIONS TO THE PES

Using the PES V^{5Z} to predict line positions does not give perfect agreement with the experiment for a variety of reasons, besides the fact that the fit does not perfectly represent the *ab initio* data. The *ab initio* data are not exact because the one-electron basis is not complete, the core electrons are not correlated, and a full CI is not used. In addition, we have neglected corrections like relativity, mass polarization, radiative, and diagonal adiabatic modifications to the Born–Oppenheimer approximation. Including all these corrections leads to a modification of the PES. In addition, there are nonadiabatic effects, which can lead to more complicated changes in our equations. Finally, there can be experimental errors. We will attempt to include these effects empirically by modifying the PES and generating a new PES called $V^{\rm emp}$, which is written in the form

$$V^{\rm emp} = c^{5Z}V^{5Z}(r_1,r_2,\theta) + c^{\rm core}\Delta V^{\rm core}(r_1,r_2,\theta) + c^{\rm basis}\Delta V^{\rm basis}(r_1,r_2,\theta) + \Delta V^{\rm rest}(r_1,r_2,\theta), \quad (10)$$

with $\Delta V^{\rm rest}$ represented by Eq. (4). The free parameters in this expression are c^{5Z}, $c^{\rm core}$, $c^{\rm basis}$, and the c_{ijk} in $\Delta V^{\rm rest}$. It should be noted that using a function of the form of Eq. (10) can only make up for some deficiencies in the fit to the original 5Z data. Errors produced by using fitting functions of the wrong form cannot be corrected. Errors that are due to nonoptimum weighting of the points can be corrected to a certain degree. That is, in this step, regions of the PES of which the eigenvalues are not sensitive will be deemphasized.

We determine the parameters in $V^{\rm emp}$ by comparing to the experimental data in the HITRAN 92 data base.[17] Since some of the corrections to the PES are mass dependent, we only consider the $H_2{}^{16}O$ isotope of water. We consider other isotopes in Sec. VIII. One problem with making this comparison is associating the theoretical lines with the appropriate experimental lines. Although most of the lines have quantum number assignments, the assignments are not always correct. In the present work, we take the assignment to consist of the rigid rotator quantum numbers[43] JK_aK_c and the internal energy for the initial and final level. Furthermore, some theoretical levels have appreciable resonance mixing, so a meaningful set of labels cannot be given (presumably this is also the case for the experimental levels). Because we use JK_aK_c and internal energy to assign transitions, resonances that do not involve K_a and K_c will not cause any difficulty. Alternatively, one can compare line positions and intensities to try and find the best match. In practice, we minimized $[(\omega^{\rm calc}-\omega^{\rm exp})/{\rm cm}^{-1}]^2+[\ln I^{\rm calc}/I^{\rm exp}]^2$ to associate lines, but this procedure is not perfect. There are instances where there are two closely spaced peaks with 3:1 intensity ratios where this procedure associates the strong peak with the weak peak (and leaves the other one unmatched) when the intensities differ greatly between experiment and theory (the 3:1 factor comes from the nuclear spin statistics). Thus, when using this method we also require that the assignments match between theory and experiment. We hope that there are enough properly assigned lines to outweigh any improperly assigned lines in the least-squares procedure. A problem with this procedure is that it excludes high-lying rovibrational levels that are not well described by a single basis function. More sophisticated pattern matching techniques would be desirable.

Another problem of more practical concern is which lines to try to match, or whether to match actual energy levels. In the present work we use lines, the motivation being that these are the directly measurable quantities. The cheapest procedure would be to just look at the R(0) lines, but

these lines are not that sensitive to the rotational energy levels. Matching all the lines is much more expensive and, furthermore, weights the rotational energy levels more than the vibrational energy levels, since for high J only rotational transitions are included in the database. In the present work, we include all lines with $J \leqslant 5$ in our optimization. For larger J, the number of vibrational transitions decreases. We will see that the potential we obtain does well for the rotational energies for higher J.

When performing least-squares optimization of potential parameters, the routine LMDER from MINPACK (Ref. 44) was used. To facilitate the optimization, the basis functions used to expand the wave functions were the low-lying eigenfunctions of the starting PES. The derivatives of the transition energies with respect to the parameters required by LMDER were computed using the Hellman–Feynman theorem for the individual eigenvalues. The most time consuming step of the optimization was the determination of the eigenvectors of the starting PES. If enough eigenfunctions are used, it is necessary to determine them only once. It appears that very accurate eigenvalues are required for the optimization process. Using poorly converged eigenvalues does not merely give the wrong PES, it causes the final errors to be larger. This apparently occurs because of the large amount of data compared to the flexibility allowed by our parameters.

The optimization was carried out in two steps. First, a preliminary fit with $c^{5Z}=1$, $c^{\rm core}=c^{\rm basis}=0$, and $\Delta V^{\rm rest}$ using $i+j+k \leqslant 2$ was carried out using the Q(1) lines, with line associations made by matching assignments. For all transitions up to 14 400 $\rm cm^{-1}$, using the *ab initio* PES (V^{5Z}), the root mean square (rms) error was 6.91 $\rm cm^{-1}$, and after the optimization, the rms error was 0.081 $\rm cm^{-1}$.

In the final optimization, the line association was made by matching peak heights and peak positions, as described above, with the theoretical calculations using the initially optimized PES. The data in the least squares fit were not equally weighted—each transition had an acceptable error associated with it. These were taken to be $\max(0.1\rm cm^{-1}, \rm err)$, where err is an estimate of the error in the theoretical calculations due to incomplete convergence of the rovibrational wave functions with respect to adding more basis functions. In addition, the weight for a few points was set to near zero if there was a large (>1 $\rm cm^{-1}$) difference between theory and experiment. A total of 5493 lines had nonzero weights, and transitions up to 20 519 $\rm cm^{-1}$ were included in the optimization (most transitions were below 17 000 $\rm cm^{-1}$). The final rms error for the 5237 points with weights equal to 1/0.1 $\rm cm^{-1}$ was 0.044 $\rm cm^{-1}$. In this fit, a total of 21 parameters were varied: three scaling the various computed functions and 18 in $\Delta V^{\rm rest}$, which included the functions $1 \leqslant i+j+k \leqslant 3$, and $k \geqslant 1$, $i+j+k \leqslant 4$. More bending functions were included because there were larger errors in the bending transitions. The parameters for $V^{\rm emp}$ are available from E-PAPS.[32]

The error as a function of the transition energy for the final fit is shown in Fig. 5. Figure 5 shows a series of clusters. Each cluster corresponds to a vibrational band, and within each cluster are the different rotational transitions.

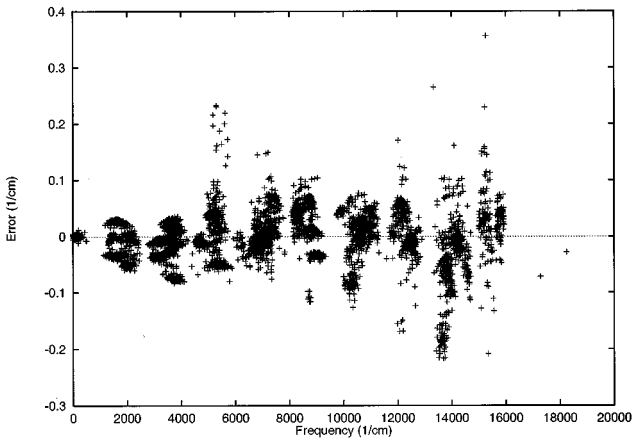

FIG. 5. Errors in line positions as a function of frequency for $J \leqslant 5$.

Many clusters show little dependence on J—they have very little vertical width. Others show fairly large scatter. The scatter increases as the transition energy increases, but the grouping of the clusters about the zero line does not change significantly. We attribute this scatter to errors in the HITRAN data base, see Sec. VII.

The fact that many vibrational transitions have errors that weakly depend on J is very important for extrapolating to higher J. In earlier fits using $c^{5Z}=1$, $c^{\rm core}=c^{\rm basis}=0$, we could not achieve this flat error. Varying these three parameters greatly improved the results. The final values of the scaling parameters were $c^{5Z}=0.999\,678$, $c^{\rm core}=1.635$, and $c^{\rm basis}=-0.159$. It can be seen that the most significant effect is from the core correction.

So far we have not explicitly included nonadiabatic effects. These are difficult to include rigorously. One simple way promoted[45] to include nonadiabaticity is to use the atomic rather than nuclear masses. In the early stages of this work, we carried out optimizations using both the atomic and nuclear masses, and in all cases the quality of the fits was not significantly different. Thus, in the final stages we only used the nuclear masses. Another way to parameterize the nonadiabatic effects is to proceed as follows;[46] for a one-dimensional problem in the electronically adiabatic representation where there are two coupled electronic states, we must solve

$$\begin{pmatrix} H_{11} & H_{12} \\ H_{21} & H_{22} \end{pmatrix} \begin{pmatrix} f_1 \\ f_2 \end{pmatrix} = E \begin{pmatrix} f_1 \\ f_2 \end{pmatrix}, \tag{11}$$

where f_i are the vibrational functions for the two states,

$$H_{ii} = -\frac{\hbar^2}{2\mu}\frac{\partial^2}{\partial r^2} + V_i(r), \tag{12}$$

V_i the PES for state i (including diagonal corrections to the Born–Oppenheimer approximation),

$$H_{12} = \frac{\hbar}{\mu} G_{12} \frac{\partial}{\partial r}, \tag{13}$$

where G_{12} is a nonadiabatic coupling matrix element, the derivative acting to the right, and

$$H_{21}=\frac{\hbar}{\mu}\frac{\partial}{\partial r}G_{12}, \tag{14}$$

with the derivative acting to the left. Since we are primarily interested in f_1, we can write the formal solution as

$$[H_{11}-H_{12}(H_{22}-E)^{-1}H_{21}]f_1=Ef_1, \tag{15}$$

thus, the nonadiabatic correction takes the form $\langle \partial f_1/\partial r\,|F|\,\partial f_1/\partial r\rangle$, where F is a nonlocal function depending on the eigenvalue. If we assume F is a constant, then this is a correction to the kinetic energy. Thus we tried to include nonadiabatic effects by introducing three scaling parameters for the kinetic energy operators, but we did not obtain significantly different results. We believe that this is not because nonadiabatic effects are small or that this is not a good way to include nonadiabatic effects, but rather that we already have included some nonadiabaticity. This can be understood by noting that we could have just as well used an electronically diabatic basis. In that case, H_{12} would include potential coupling but no derivative coupling, and the nonadiabatic correction would just change the PES. One conformation of this notion is the fact that when fewer parameters were used in $\Delta V^{\rm rest}$, scaling the kinetic energy operators did improve the results. However this change, as well as the kinetic energy scaling, should in principle be different for each rovibrational level.[47] Thus, by using a single PES or single set of kinetic energy scaling parameters, we can only hope to mimic the nonadiabatic effect on the average. It should be noted that in our calculations, scaling the kinetic energy operators is not equivalent to changing the masses because there are three scaling parameters and only two unique masses, and the masses also enter in the definition of the internal coordinates.

One other observation on the nuclear versus atomic mass question is as follows: For water, the choice of the mass of oxygen is not critical.[37] Suppose we scale the atomic coordinates by the factor $s^{1/2}$, then the resulting Schrödinger equation will involve the scaled masses m_i/s, where m_i is the mass of atom i. To evaluate the PES, one would have to unscale the coordinates. Now one could introduce an empirical correction to the PES that would exactly cancel this scaling, thus scaling the coordinates everywhere, except in the PES, represents a change to the PES. If we take s to be equal to the ratio of the hydrogen nuclear-to-atomic mass, and the results are not sensitive to the difference between the oxygen atomic mass and s times the oxygen nuclear mass, then the computed rovibrational energies from an empirically determined PES will not depend on the choice of mass if the empirical correction is sufficiently flexible. We have tried calculations using atomic masses and scaling the coordinates in $V^{\rm emp}$, and we find a shift of 0.036 $\rm cm^{-1}$ to the zero point energy and a 0.02 $\rm cm^{-1}$ change in the fundamentals. Thus, it appears that the choice of mass is important only if the errors are of this order. Thus, in retrospect, it would have been worthwhile considering trying the atomic masses in the final fit.

Another complication arises due to coupling between electronic and nuclear angular momentum. This will lead to corrections to the rotational kinetic energy, and the derivation of Ref. 46 shows terms scaling as J^4. Although the trend is for the errors to increase with J, the increase is not dramatic, so these terms are apparently small.

VII. DISCUSSION OF THE RESULTS OBTAINED FOR $H_2{}^{16}O$ FOR THE EMPIRICAL PES.

Using the final PES $V^{\rm emp}$, we have performed calculations up to $J=55$ in order to generate a high temperature line list. This produced 307 721 352 lines. To obtain this line list, contact the authors.[48] We now compare these results to the complete HITRAN 96 database. To associate the theoretical and tabulated lines, we used the following procedure. This involves several steps because of different ambiguities in the line assignments. We only used the 289 806 theoretical lines with intensities greater than 10^{-30} cm/molecule at 296 K in the automated matching procedure.

In the theoretical results, there are two nearly degenerate levels that both have the dominant configuration $010\,13_{11\,2}$. These levels differ in energy by only 0.02 $\rm cm^{-1}$, and transitions into either level have about the same intensity, which is about half the intensity of the single lines contained in the database. Thus, before matching the lines, we replaced the pair of lines with a single one using the average position and the sum of the intensities.

In the first step of the matching, for each line in the database, we searched the theoretical lines for a transition with the same assignments for the initial and final levels. This used a 30 $\rm cm^{-1}$ window. Once a theoretical line was matched with a line from the database, it was taken out of the pool of available lines. In the second matching step, we allow for resonant mixing between the rotational and vibrational quantum numbers of the final level. Thus, we proceed as before except we ignore K_a and K_c of the final level, and we use a 2 $\rm cm^{-1}$ window. Next we do the same, but allow for resonant mixing only in the initial level. There are a number of lines in the database that appear to have missassigned vibrational energies. We match these next by proceeding as in the first step except we ignore the internal energy when matching assignments and only accept a match if the intensities agree within a factor of 10. There are a number of unassigned lines in the database, and we match them by minimizing $[(\omega^{\rm calc}-\omega^{\rm exp})/\rm cm^{-1}]^2+[\ln I^{\rm calc}/I^{\rm exp}]^2$. In many cases, the match of the unassigned lines was very clear. In the final automated step, we repeated the first step, but used a 101 $\rm cm^{-1}$ window. This was done because there are several lines for which the hundreds digit of the line position is in error by one. Then about a dozen lines were matched by hand. Mostly this involved extracting a line from the theoretical results with an intensity less than the 10^{-30} cm/molecule cutoff, but in a couple of cases additional missassigned lines were matched. By this means, 30 092 of the 30 117 lines were matched. Of the remaining lines, all but one were very weak and so could not be unambiguously matched. The other line was sufficiently distant from theo-

TABLE IV. Comparison between HITRAN 96 and results from V^{emp} by vibrational bands. Frequencies are in cm^{-1} and intensity in cm/molecule.

			Line positions				Intensities[a]		
			Error percentiles						
Band	No. Lines	No. Outliners	25%	50%	75%	Max. abs. error	Summed HITRAN	Summed ratio	Max. ratio
010 010	752	23	−0.01	0.00	0.00	0.71	2.22(−20)[b]	1.02	2.1(0)
000 000	1728	26	−0.01	0.00	0.01	0.80	5.27(−17)	1.01	4.2(2)
020 020	129	3	0.00	0.00	0.00	0.02	1.01(−23)	1.10	1.7(0)
010 000	1770	20	−0.01	0.01	0.02	0.76	1.06(−17)	1.08	4.1(4)
020 010	726	17	−0.05	−0.04	−0.03	0.45	9.71(−21)	0.98	4.9(0)
100 010	402	2	−0.04	−0.04	−0.04	0.06	1.82(−22)	0.83	2.7(1)
030 020	121	1	−0.01	0.00	0.00	0.02	5.12(−24)	1.25	1.7(0)
001 010	365	3	0.00	0.01	0.02	0.05	2.63(−22)	0.95	4.3(0)
020 000	1126	47	−0.03	−0.01	0.00	4.64	7.57(−20)	1.18	7.7(2)
030 010	314	14	−0.05	−0.04	−0.03	0.88	7.28(−23)	1.19	2.1(0)
100 000	1301	27	−0.04	−0.03	−0.02	0.43	4.95(−19)	1.28	6.6(2)
001 000	1546	34	0.01	0.03	0.04	0.26	7.20(−18)	1.16	8.6(0)
110 010	370	1	−0.01	0.01	0.02	0.07	2.13(−22)	1.18	1.6(0)
011 010	521	6	−0.07	−0.06	−0.06	0.09	2.90(−21)	1.27	1.4(0)
030 000	665	18	−0.16	−0.02	−0.01	46.48	4.02(−22)	1.60	2.7(3)
110 000	997	8	−0.02	0.01	0.03	62.24	4.18(−20)	1.10	3.8(5)
011 000	1297	9	−0.05	−0.04	−0.04	25.65	8.00(−19)	1.13	2.9(2)
021 010	285	14	0.03	0.06	0.08	0.80	6.58(−22)	1.06	7.8(0)
040 000	215	9	−0.04	−0.02	0.01	34.16	1.77(−23)	1.18	2.2(4)
021 000	958	52	−0.03	−0.01	0.03	70.49	3.81(−20)	1.03	9.1(3)
120 000	613	32	−0.05	−0.03	−0.01	19.96	2.46(−21)	1.09	6.6(7)
200 000	988	33	−0.06	−0.01	0.01	23.58	6.11(−20)	1.35	7.0(5)
101 000	1325	63	−0.02	0.00	0.02	100.14	5.63(−19)	0.94	2.5(5)
002 000	886	43	0.02	0.06	0.08	14.77	3.65(−21)	1.28	2.7(4)
130 000	263	10	−0.01	0.01	0.04	1.50	4.42(−22)	1.14	2.7(2)
031 000	330	1	0.04	0.06	0.08	91.94	1.28(−21)	0.38	3.8(3)
111 000	596	6	−0.02	0.00	0.01	58.70	3.54(−20)	1.33	3.3(5)
210 000	237	6	0.02	0.05	0.07	17.53	1.48(−21)	1.18	6.2(3)
012 000	364	8	−0.04	−0.03	−.03	1.43	7.54(−22)	1.19	1.6(2)
041 000	163	2	0.04	0.05	0.06	10.10	3.03(−23)	7.17	1.2(2)
121 000	401	13	−0.10	−0.08	−0.05	7.04	2.15(−21)	1.80	1.1(2)
220 000	119	2	−0.05	−0.03	−0.02	0.52	1.29(−22)	0.62	1.7(5)
300 000	736	22	−0.03	−0.01	0.01	25.41	2.62(−21)	0.78	4.9(4)
201 000	583	9	−0.01	0.01	0.02	12.94	1.70(−20)	0.96	3.0(3)
003 000	402	6	0.02	0.05	0.06	0.11	1.90(−21)	1.14	8.8(3)
131 000	231	14	0.00	0.01	0.91	100.00	3.76(−23)	0.20	3.0(6)
211 000	450	18	0.00	0.03	0.05	10.22	1.20(−21)	1.31	1.8(1)
310 000	407	21	−0.07	−0.02	0.03	8.45	8.99(−23)	1.40	1.1(4)
013 000	250	23	−0.02	−0.01	0.00	3.81	8.78(−23)	0.77	1.7(2)
221 000	295	17	−0.22	−0.18	−0.12	3.63	1.72(−22)	2.20	5.4(0)
301 000	659	25	−0.09	−0.05	0.05	15.71	1.28(−21)	0.91	2.6(1)
320 000	253	10	−0.20	−0.11	−0.06	2.43	2.03(−23)	1.14	5.7(1)
302 000	160	8	−0.14	−0.09	0.58	18.08	2.25(−23)	0.56	1.6(2)
400 000	390	9	−0.10	−0.04	−0.02	12.81	1.06(−22)	0.88	4.5(2)
231 000	111	1	−0.01	0.01	0.06	14.81	5.76(−24)	0.56	7.5(1)
311 000	339	17	−0.11	−0.06	0.05	5.93	1.03(−22)	1.10	6.9(0)
312 000	136	9	−0.14	−0.10	0.02	4.86	1.54(−23)	0.76	2.5(3)
401 000	359	12	−0.16	0.12	1.05	35.42	8.21(−23)	0.92	5.4(1)
402 000	148	7	−0.39	−0.16	0.51	7.77	2.24(−23)	0.34	1.1(4)
321 000	200	3	−0.47	−0.30	−0.13	73.32	4.60(−23)	1.14	8.5(2)
500 000	115	4	−0.20	−0.18	−0.02	15.58	3.99(−24)	0.74	2.8(1)
411 000	107	2	−0.04	0.12	0.66	5.27	2.79(−24)	1.37	8.0(0)

[a]The theoretical intensities are multiplied by the isotope abundance factor 0.997 32.
[b]$2.22(-20)=2.22\times10^{-20}$.

retical lines of similar strength to make a match difficult.

In Table IV, we give a band-by-band comparison of the present results and those from the database. In Table IV we only include the bands with at least 100 lines. This includes 28 204 out of the 30 092 matched lines. We measure the errors in the line positions by giving the 25, 50, and 75 percentiles of $\omega^{calc}-\omega^{exp}$ as well as the maximum $|\omega^{calc}-\omega^{exp}|$. For example, for the 000 000 band, 25% of the

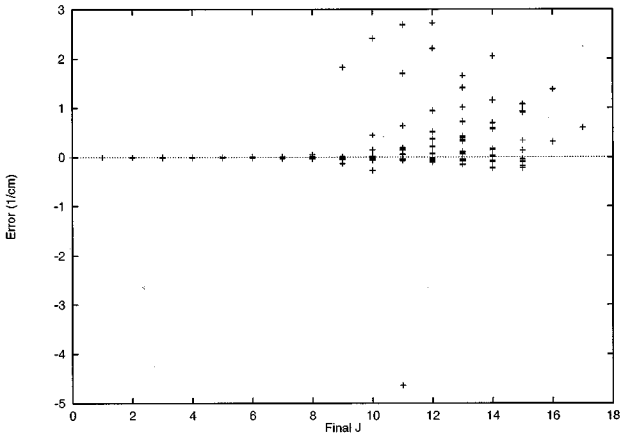

FIG. 6. Errors in transition frequency for 020←000 band as a function of final J. There are 1126 points shown.

$\omega^{\mathrm{calc}}-\omega^{\mathrm{exp}}$ are more negative than -0.01 cm^{-1}, the median difference is 0.00 cm^{-1}, and 25% of the lines have $\omega^{\mathrm{calc}}-\omega^{\mathrm{exp}}$ greater than 0.01 cm^{-1}. We do not find it useful to quote the rms error, because there are a number of outliers for each band, and they distort the rms error. For example, for this band the maximum error is 0.80 cm^{-1}, and we consider 26 of the 1728 lines to be outliers. We determine the outliers by computing the average absolute deviation from the average. Then lines with errors greater than four times this are considered outliers. Using three times the average absolute deviation from the average produces very similar results because there is usually a big gap between the outliers and the other lines. We use the average absolute deviation from the average rather than the rms error, because it is more well behaved in the presence of outliers.[49] About 3% of the lines are outliers.

Some of the outliers appear to be due to transcription errors somewhere in the preparation of the database. For example, the 101 000 band has four lines with errors very close to 100 cm^{-1}, the 131 000 band has one line with an error very close to 100 cm^{-1}, and the 041 000 band has two lines with errors very close to 10 cm^{-1}. The 211 000 band has one line with an error very close to 10 cm^{-1}. Otherwise, the errors for these bands is usually quite small, thus, it seems very likely that one digit is off by one unit for these lines. Other transcription errors, like transposed digits or errors in the units digit or to the right of the decimal point are less obvious. We note that there are many lines with errors very close to 1 cm^{-1}. We have tried to see if there were any trends with the outliers, and so we plotted their errors for many bands as a function of various quantities. A typical example is Fig. 6, where we plot the errors for the 020 000 band as a function of the final value of J for the line. We see many points having very small errors, randomly scattered points with large errors, and then points with errors increasing at high J. The outliers only occur for $J\geqslant 9$ for this band. This suggests that in addition to transcription errors, some of the outliers are due to missassignments of weak lines having high J due to inadequacies of the model Hamiltonians used in the line analysis. However, we cannot rule out the possibility of errors in our Hamiltonian which become important at higher J. Also, recall that we only used $J\leqslant 5$ when optimizing our potential, thus optimizations using higher J could reduce the errors at high J. However, given the presence of the outliers, it is not clear which lines should be included in the fit at high J. Considering the errors as a function of K_a and K_c did not reveal further insight into the sources of the errors.

Returning now to Table IV, we see that most bands are fit very well. The agreement deteriorates at the highest frequency transitions, but remains quite good. Some of the increase in error may be due to incomplete convergence of the rovibrational wave-function expansions. Overall, the errors are small: for all 30 092 lines, 5% have $\omega^{\mathrm{calc}}-\omega^{\mathrm{exp}}$ more negative than -0.40 cm^{-1}, 10% more negative than -0.11 cm^{-1}, 25% more negative than -0.04 cm^{-1}, the median error is -0.008 cm^{-1}, 25% have differences greater than 0.02 cm^{-1}, 10% greater than 0.07 cm^{-1}, and 5% greater than 0.38 cm^{-1}.

It would be interesting to compare our computed line positions to recent analysis of flame studies,[50,51] but as we do not have electronic versions of that data, we do not make such a comparison here.

Also included in Table IV is a comparison of line intensities. Here, we do not include the outliers. We give the intensity summed over all lines in the band from HITRAN 96, and the ratio of the summed intensity from the calculations to the summed intensity from HITRAN. For most bands, there is good agreement. Out of the 52 bands, 15 have ratios between 0.9 and 1.1, and 29 have ratios between 0.8 and 1.2. All but five agree within a factor of 2, with the largest deviation being a factor of 7.17 for the 041 000 band. For this band, the theoretical lines are systematically stronger than those in the database. The agreement for individual line strengths is not always so good, even for bands where the summed intensity agrees well. We also give in Table IV the maximum of $I^{\mathrm{calc}}/I^{\mathrm{exp}}$ and $I^{\mathrm{exp}}/I^{\mathrm{calc}}$. This can be as large as 6.6×10^{7}, which occurs for the 120 000 band—here the summed intensities agree within 10%. It is likely that there are transcription errors in the intensities as well. Missassignments of lines may also contribute to the errors.

It is important to note that many of the intensities in the HITRAN data base are not obtained from measurement but rather from approximate theoretical calculations parameterized by other measurements, thus some disagreement with the present results is not unexpected. In Fig. 7, we show the intensity in absorption for room temperature $H_2{}^{16}O$ computed using the HITRAN 92 database and the present PES and DMS. In generating the spectra, a Gaussian of full width at half-maximum of 20 cm^{-1} was used for each line. The spectrum shows a series of peaks separated by deep valleys. The peaks agree quite well, however, there are greater differences in the valleys. Part of this is because the present results include many more weak lines.

It is one thing to obtain accurate line positions, but another to also get accurate rovibrational energies. We have compared the rovibrational energies for $J=20$ obtained from

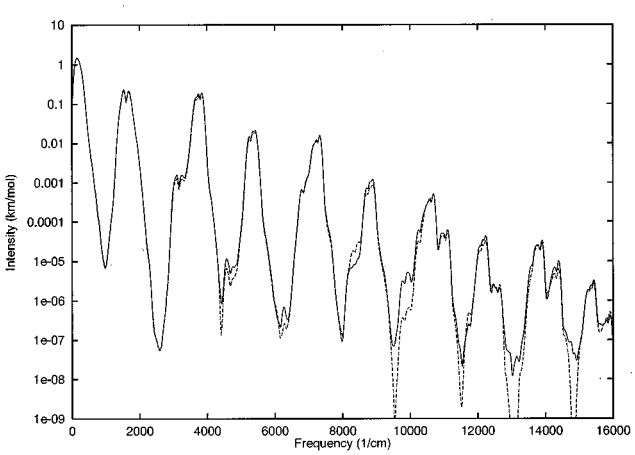

FIG. 7. Room temperature intensities for $H_2{}^{16}O$. Solid line, present results, dashed line, HITRAN 92 database.

V^{emp} with those given for the Polyansky–Jensen–Tennyson (PJT) potential.[9] These are given in Table V. The maximum difference between experiment and the present work is 0.15 cm^{-1}, and we obtain errors smaller than PJT 25 times out of the 35 cases where experimental data is available. The root-means-square deviation between theory and experiment is 0.15 cm^{-1} for the PJT PES and 0.07 cm^{-1} for V^{emp}. Thus, the present PES gives very accurate rovibrational energies for high J as well.

In Table VI we give energy levels up to about 16 000 cm^{-1} above the zero point energy for $J=0$ obtained using V^{emp}. In the second column we give the difference between the HITRAN 96 energies and those we have calculated. The agreement is very good, mostly with errors much smaller than 0.1 cm^{-1}. The largest error is for the level at 12 139 cm^{-1}, which is a mixture of the 310 and 112 levels, where the difference is 0.49 cm^{-1}. The other mixture of 310 and 112 has an error of only 0.01 cm^{-1}. Thus it may be possible that the tabulated energy is wrong. Note also that the band labeled 310 000 in Table IV gives very good results. Of the 43 levels where data is available from HITRAN, only five have errors bigger than 0.1 cm^{-1}. It is interesting to compare our prediction of the 050 level, 7542.51 cm^{-1}, with the recent experimental[50] value of 7542.39 ± 0.05 cm^{-1}. The agreement is quite good.

Also included in Table VI is the entropy of mixing[36] and the wave-function decomposition from a natural modal analysis of each level. The quantum number labels were determined as before[52] by node counting, followed by readjustment in selected cases. Thus, the labels are not infallible, especially for weakly occupied components. This happens since a single set of functions for all levels is not used. As the energy increases, the amount of mixing increases, except for certain isolated cases, such as the 0 11 0 level. The mixing is usually of two types. There is strong mixing between levels that do not change $\nu_1+\nu_3$, which is well known for H_2O. There is also stretch–bend mixing between the levels $\nu_1\nu_2\nu_3$ and $\nu_1+1\,\nu_2-n\,\nu_3$ with $n=2$ for low ν_2 and $n=3$ for higher ν_2. As anharmonicity changes the optimum value of n, so some high bending levels can be quite pure, e.g., the 0 11 0 level.

TABLE V. Rotational energy levels for $H_2{}^{16}O$, $J=20$ (in cm^{-1}).

K_a	K_c	exp.[a]	PJT[a]	V^{emp}
0	20	4048.252	4048.285	4048.35
1	20	4048.252	4048.285	4048.35
1	19	4412.317	4412.335	4412.41
2	19	4412.317	4412.335	4412.41
2	18	4738.624	4738.623	4738.70
3	18	4738.636	4738.634	4738.71
3	17		5031.77	5031.86
4	17	5031.977	5031.968	5032.05
4	16	5292.096	5292.056	5292.16
5	16	5294.035	5293.995	5294.09
5	15	5513.266	5513.146	5513.28
6	15	5527.046	5526.980	5527.09
6	14		5680.64	5680.81
7	14	5739.23	5739.15	5739.27
7	13		5811.92	5812.09
8	13	5947.33	5947.25	5947.35
8	12		5966.72	5966.86
9	12	6167.91	6167.68	6167.75
9	11	6170.96	6170.80	6170.87
10	11		6407.09	6407.12
10	10		6407.45	6407.49
11	10	6664.14	6664.20	6664.18
11	9	6664.17	6664.23	6664.21
12	9	6935.42	6935.53	6935.46
12	8	6935.43	6935.54	6935.46
13	8	7217.56	7217.71	7217.59
13	7	7217.56	7217.71	7217.59
14	7	7507.57	7507.77	7507.60
14	6	7507.57	7507.77	7507.60
15	6	7802.7	7802.9	7802.70
15	5	7802.7	7802.9	7802.70
16	5	8100.3	8100.5	8100.27
16	4	8100.3	8100.5	8100.27
17	4	8397.6	8397.9	8397.59
17	3	8397.6	8397.9	8397.59
18	3	8691.9	8692.1	8691.84
18	2	8691.9	8692.1	8691.84
19	2	8979.8	8980.0	8979.75
19	1	8979.8	8980.0	8979.75
20	1	9257.408	9257.416	9257.29
20	0	9257.408	9257.416	9257.29

[a]From Ref. 9.

In Table VII we give some selected dipole matrix elements, which should be useful for users of the PES and DMS given in the present work. The tabulated quantity is the square of the matrix element of the dipole moment, averaged over initial-state rotational degeneracies and summed over final-state rotational degeneracies. When available, the results from the HITRAN 92 database are also given. The agreement between the calculated and HITRAN 92 frequencies is very good, while the agreement of the matrix elements is less satisfying.

As mentioned above, we have carried out calculations of a high-temperature line list for $H_2{}^{16}O$ using V^{emp} and the DMS of this work. Calculations were carried out for J up to 55 and a total of 170 625 rovibrational energy levels were determined. The maximum number of roots extracted per

TABLE VI. Energy levels and wave function components for $H_2{}^{16}O$, $J=0$.

Energy (cm^{-1})	o−c[a]	Entropy	ν_1	ν_2	ν_3	Coef	ν_1	ν_2	ν_3	Coef	ν_1	ν_2	ν_3	Coef
						Even levels								
0.00	0.00	0.01	0	0	0	1.00	1	0	2	0.02	1	1	0	0.01
1594.78	−0.03	0.02	0	1	0	1.00	1	0	0	0.02	1	1	2	0.02
3151.63	0.00	0.08	0	2	0	1.00	1	0	0	−0.08	1	2	2	0.02
3657.04	0.01	0.12	1	0	0	1.00	0	2	0	0.06	0	0	2	0.06
4666.79	0.00	0.15	0	3	0	0.99	1	1	0	−0.11	1	3	2	0.02
5235.03	−0.05	0.19	1	1	0	0.99	0	3	0	0.10	0	1	2	0.06
6134.04	−0.03	0.21	0	4	0	0.99	1	2	0	−0.14	1	4	2	0.02
6775.10	−0.01	0.36	1	2	0	0.98	0	4	0	0.13	2	2	0	−0.10
7201.55	−0.01	0.86	2	0	0	0.93	0	0	2	0.35	1	2	0	0.08
7445.12	−0.07	0.78	0	0	2	0.94	2	0	0	−0.34	1	0	4	0.04
7542.51		0.25	0	5	0	0.99	1	3	0	0.16	0	4	2	−0.02
8274.05	−0.07	0.51	1	3	0	0.97	2	1	0	−0.18	0	4	0	−0.13
8761.66	−0.08	1.01	2	1	0	0.92	0	1	2	0.35	1	3	0	0.12
8870.59		0.29	0	6	0	0.98	1	5	0	0.17	0	3	2	−0.03
9000.11	0.03	0.84	0	1	2	0.93	2	1	0	−0.35	1	3	0	−0.05
9724.40		0.66	1	4	0	0.96	2	2	0	−0.22	0	3	0	−0.15
10 087.15		0.36	0	7	0	0.98	1	5	0	−0.19	2	3	0	−0.04
10 284.35	0.02	1.28	2	2	0	0.90	0	2	2	0.35	3	4	0	−0.16
10 521.77		0.99	0	2	2	0.93	2	2	0	−0.34	1	0	2	−0.08
10 599.68	0.01	1.64	3	0	0	0.75	1	0	2	0.64	0	0	4	0.10
10 868.89	0.01	1.63	1	0	2	−0.75	3	0	0	0.64	0	0	4	−0.12
11 099.24		1.32	1	5	0	0.88	0	8	0	0.43	2	3	0	0.20
11 254.40		1.10	0	8	0	0.90	1	5	0	−0.42	2	4	0	−0.11
11 767.52		1.47	2	3	0	0.89	0	3	2	0.34	3	1	0	−0.21
12 007.92		1.09	0	3	2	0.92	2	3	0	−0.33	1	1	2	−0.11
12 139.36	−0.49	1.83	3	1	0	0.73	1	1	2	0.63	1	3	2	0.11
12 381.94		1.69	1	6	0	0.71	0	9	0	0.68	2	4	0	0.16
12 407.65	0.01	1.84	1	1	2	−0.73	3	1	0	0.64	0	1	4	−0.12
12 533.66		1.68	0	9	0	0.73	1	6	0	−0.65	2	5	0	−0.18
13 205.14		1.57	2	4	0	0.88	0	4	2	0.31	3	2	0	−0.25
13 453.71		1.17	0	4	2	0.92	2	4	0	−0.30	2	2	2	−0.12
13 640.58		2.43	3	2	0	0.68	2	2	2	0.58	3	2	2	0.17
13 661.61		1.77	1	7	0	0.85	0	10	0	−0.40	2	6	0	0.24
13 828.16	0.12	1.98	2	0	2	0.80	4	0	0	0.49	1	0	4	0.29
13 857.46		1.08	0	10	0	0.91	1	7	0	0.40	2	6	0	−0.11
13 910.79	0.11	2.13	1	2	2	−0.71	3	2	0	0.62	4	4	0	−0.12
14 221.13	0.03	1.88	4	0	0	0.82	2	0	2	−0.41	1	0	4	−0.35
14 537.42		1.22	0	0	4	0.90	2	0	2	−0.40	4	0	0	0.17
14 579.47		1.71	2	5	0	0.87	1	4	0	0.27	1	5	2	0.23
14 819.82		2.52	1	8	0	0.61	1	5	2	−0.48	0	5	2	−0.41
14 881.86		2.72	1	5	2	0.47	0	5	2	−0.42	1	8	0	−0.38
15 108.15		2.46	3	3	0	0.68	2	3	2	0.59	2	1	2	−0.19
15 295.36		0.55	0	11	0	0.97	1	1	0	0.25	2	7	0	−0.05
15 344.41	0.09	2.26	2	1	2	0.79	4	1	0	0.43	1	1	4	0.29
15 377.79		2.46	1	3	2	−0.71	3	3	0	0.56	4	1	0	−0.25
15 742.79	0.01	2.12	4	1	0	0.81	2	1	2	−0.39	1	1	4	−0.34
15 871.18		2.03	2	6	0	0.80	1	9	0	0.49	3	4	0	0.24
16 046.92		1.33	0	1	4	0.89	2	1	2	−0.40	4	1	0	0.17
						Odd levels								
3755.96	−0.03	0.02	0	0	1	1.00	1	0	3	0.04	0	1	3	0.01
5331.22	−0.05	0.04	0	1	1	1.00	1	1	3	0.04	1	0	1	0.02
6871.50	0.02	0.12	0	2	1	0.99	1	0	1	−0.09	1	2	3	0.04
7249.86	−0.04	0.22	1	0	1	0.99	0	0	3	0.12	0	2	1	0.07
8373.90	−0.05	0.21	0	3	1	0.99	1	1	1	−0.13	1	3	3	0.04
8807.04	−0.04	0.31	1	1	1	0.98	0	3	1	0.11	0	1	3	0.11
9833.63	−0.04	0.28	0	4	1	0.99	1	2	1	−0.16	1	4	3	0.04
10 328.67	0.06	0.54	1	2	1	0.97	2	2	1	−0.12	0	2	3	0.11
10 613.40	−0.05	0.96	2	0	1	0.92	0	0	3	0.37	1	2	1	0.09
11 032.46	−0.05	0.81	0	0	3	0.93	2	0	1	−0.35	1	0	5	0.05
11 242.78		0.33	0	5	1	0.98	1	3	1	0.18	0	4	3	−0.04
11 813.23	−0.02	0.72	1	3	1	0.96	2	1	1	−0.21	0	5	1	−0.15
12 151.32	−0.07	1.14	2	1	1	0.91	1	1	3	0.37	1	3	1	−0.13
12 565.01	0.00	0.88	1	1	3	0.93	2	1	1	−0.35	1	1	5	0.05
12 586.33		0.37	0	6	1	0.98	1	4	1	0.19	0	5	3	−0.05

TABLE VI. (*Continued*.)

Energy (cm^{-1})	o−c[a]	Entropy	ν_1	ν_2	ν_3	Coef	ν_1	ν_2	ν_3	Coef	ν_1	ν_2	ν_3	Coef
						Even levels								
13 256.25		0.84	1	4	1	0.95	2	2	1	−0.24	0	5	1	−0.15
13 652.46	0.20	1.54	2	2	1	0.88	0	2	3	0.36	3	2	1	−0.19
13 830.84	0.10	1.76	3	0	1	0.79	2	0	3	0.56	2	2	1	0.12
13 835.85		0.51	0	7	1	0.97	1	6	1	−0.19	3	0	1	0.07
14 066.21	0.02	1.05	0	2	3	0.92	2	2	1	−0.34	1	0	3	−0.07
14 318.75	0.06	1.67	1	0	3	0.79	3	0	1	−0.57	0	0	5	0.17
14 648.19		0.97	1	5	1	0.94	2	3	1	0.27	0	4	1	0.18
14 984.72		0.52	0	8	1	0.97	1	7	1	0.21	2	4	1	−0.08
15 119.03	0.00	1.80	2	3	1	0.85	0	3	3	0.35	3	1	1	−0.26
15 347.85	0.11	1.93	3	1	1	0.77	1	1	3	0.56	2	3	1	−0.17
15 534.83		1.19	0	3	3	0.92	2	3	1	−0.33	3	1	1	0.10
15 832.68	0.08	1.85	1	1	3	0.78	3	1	1	−0.57	0	1	5	0.16
15 969.61		1.37	1	6	1	0.89	0	9	1	0.36	2	4	1	0.24
16 160.69		1.00	0	9	1	0.92	1	6	1	−0.35	2	5	1	−0.12
16 546.44		1.89	2	4	1	0.84	1	4	3	0.33	3	2	1	−0.30

[a]Difference between HITRAN 96 energy and calculated energy in cm^{-1}.

JPS was 1633, and that occurred for $JPS=17--$. A total of 307 721 352 possible transitions are generated by the computed levels, and the line strengths for each line have been calculated. In Fig. 8 we show the computed line strengths in absorption for several temperatures. At high temperature, the dips between the vibrational bands have almost completely filled in. The partition function computed from these energy levels is given in Table VIII. We use statistical weights of 1 and 3 for the different symmetries. The partition function may be fit by a power series in temperature using half integral powers.

These calculations were designed to be the best that could be carried out given the algorithm used and the computer hardware available. The high-lying levels are not well converged, but it is expected that this line list will be valuable for high-temperature simulations because the poorly converged levels will primarily contribute to weak lines that form an unresolved background to the spectra.

VIII. OTHER ISOTOPES

In this section we consider the other isotopes. Table IX gives low lying vibrational frequencies for seven different isotopically substituted water molecules. The first line gives the frequency determined using the PES V^{emp}, the second using the PES V^{mass} described below, the third uses an *ab initio* diagonal adiabatic correction,[37] and the fourth is the experimental value.[53–59] First consider the different oxygen isotopes of H_2O. The agreement between the results obtained using V^{emp} and the experiment is very good: the maximum difference is only 0.03 cm^{-1}. Thus we used V^{emp} to generate line lists for $H_2{}^{17}O$ and $H_2{}^{18}O$ to compare to the lines in the HITRAN 96 database for these isotopically substituted species. These calculations used parameter set A of Sec. V. In Tables X and XI we give the band by band comparison between the

TABLE VII. Selected dipole matrix elements.

Transition		Frequency (cm^{-1})		Matrix Element ($Debye^2$)	
$\nu_1\nu_2\nu_3$	$\nu_1\nu_2\nu_3$	Calc.	HITRAN	Calc.	HITRAN
			$1_{11}\leftarrow 0_{00}$		
0 0 0	0 0 0	37.138	37.137 08	3.479	3.454
0 1 0	0 0 0	1634.999	1634.967 10	1.663(−2)[a]	1.497(−2)
0 2 0	0 0 0	3196.092	3196.093 00	6.264(−5)	4.875(−5)
1 0 0	0 0 0	3693.280	3693.293 90	2.520(−4)	1.756(−4)
			$1_{01}\leftarrow 0_{00}$		
0 0 1	0 0 0	3779.530	3779.492 90	5.508(−3)	4.713(−3)
			$1_{10}\leftarrow 1_{01}$		
0 0 1	0 0 1	17.475		1.783	
0 1 1	0 0 1	1595.785		8.044(−3)	
0 2 1	0 0 1	3140.021		3.390(−5)	
1 0 1	0 0 1	3510.489		1.035(−4)	
			$1_{11}\leftarrow 1_{10}$		
1 0 1	1 0 0	3586.291		2.550(−3)	

[a]$1.663(-2)=1.663\times 10^{-2}$.

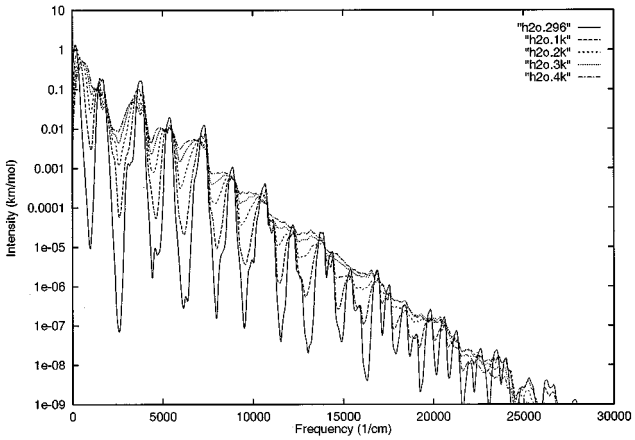

FIG. 8. Spectra of $H_2{}^{16}O$ for several temperatures.

calculated and tabulated results. Tables X and XI use the same format as Table IV, and again we only give results for bands with at least 100 lines.

The results in Table X for $H_2{}^{17}O$ are quite similar to the results for $H_2{}^{16}O$. Most of the bands are fit very well, with the exceptions of the 111 and 201 bands, which differ systematically by nearly 3/4 cm^{-1}. The calculated frequencies are too low. These are fairly high-energy transitions and may be hinting that a mass dependent correction is beginning to be important. Overall, the 5, 10, 25, 50, 75, 90, and 95 percentile differences between the calculated and tabulated line positions are -1.17, -0.75, -0.03, -0.02, 0.02, 0.03, and 0.04 cm^{-1}. About 2.4% of the lines appear to be outliers. There are a total of 3744 lines in the database for this species, and we were able to match all the tabulated lines with calculated lines. The agreement between the calculated and tabulated intensities is usually quite good.

In Table XI we give the results for $H_2{}^{18}O$. Again the results are very good on the whole, with a few bands systematically off: the 012 band is about 3 cm^{-1} too low, the 031 band is about 4 cm^{-1} too low, and the 003 band is about 6 cm^{-1} too low. The 111 and 201 bands that were systematically too low for $H_2{}^{17}O$ are now a little too high. If the difference was due primarily to a correction to the PES that scales with the mass of the oxygen atom, then we would expect the ^{17}O results to be intermediate between ^{16}O and ^{18}O, which is not what we observe. Perhaps some experimental error is involved in these bands. Out of the 6357 lines for this species, we were able to match all but one with calculated lines, and the 5, 10, 25, 50, 75, 90, and 95 percentile differences between the calculated and tabulated line positions are -2.98, -0.06, -0.03, 0.00, 0.03, 0.20, and 0.43 cm^{-1}. We estimate that about 3.4% of the lines are outliers. The intensities agree pretty well between the computed and tabulated results.

TABLE VIII. Partition function for water.

Temperature(K)	$H_2{}^{16}O$
5	1.009 678 1
10	1.328 362 2
50	12.961 455
75	23.170 043
100	35.152 775
200	97.413 639
296	174.578 18
500	386.322 23
750	739.067 20
1000	1218.2469
1500	2713.0010
2000	5276.1830
2500	9455.0113
3000	15 949.203
3500	25 606.465
4000	39 371.543

Now return to Table IX and consider $HD^{16}O$, the only other water species for which data exists in the HITRAN database. Here, the differences between the frequencies from $V^{\rm emp}$ and the database are larger — up to 0.26 cm^{-1}. In fact, if one considers all 2058 lines in the database with $J \leqslant 5$, the rms difference between the frequencies computed using $V^{\rm emp}$ and the HITRAN 96 database is 0.247 cm^{-1}, which is about a factor of 6 times greater than for $H_2{}^{16}O$. There is also extensive data[54,59] for $D_2{}^{16}O$ and if we generate lines from the 180 tabulated energies with $J \leqslant 5$, the rms error using $V^{\rm emp}$ is 0.182 cm^{-1} for the 2133 lines with computed intensities greater than 10^{-30} cm/molecule (without including an isotope abundance factor). To improve on this, we decompose the PES into a mass independent part, called $V^{\rm BO}$, and a correction, $\Delta V^{\rm Ad}$, divided by the hydrogen masses. $V^{\rm BO}$ should represent the Born–Oppenheimer PES plus relativistic and any mass independent effective nonadiabatic corrections, while $\Delta V^{\rm Ad}$ should represent the diagonal adiabatic correction to the Born–Oppenheimer PES, mass polarization corrections, and any effective nonadiabatic corrections that scale as the inverse of the mass. Specifically, we write

$$V^{\rm mass}(r_1,r_2,\theta)=V^{\rm BO}(r_1,r_2,\theta)+\frac{1}{m_1}\Delta V^{\rm Ad}(r_1,r_2,\theta)+\frac{1}{m_2}\Delta V^{\rm Ad}(r_2,r_1,\theta), \tag{16}$$

where m_i is the mass of the ith hydrogen isotope in the water molecule and $V^{\rm BO}$ and $\Delta V^{\rm Ad}$ are determined by requiring that $V^{\rm mass}=V^{\rm emp}$ for $H_2{}^{16}O$, $V^{\rm mass}=V^{\rm emp}+\Delta V^{\rm HDO}$ for $HD^{16}O$, and $V^{\rm mass}=V^{\rm emp}+\Delta V^{\rm D_2O}$ for $D_2{}^{16}O$, where $\Delta V^{\rm HDO}$ and $\Delta V^{\rm D_2O}$ are corrections added to $V^{\rm emp}$ to match the experiment for these species. We can parameterize these with a single set of coefficients because

$$\Delta V^{\rm HDO}(r_1,r_2,\theta)=\left(\frac{1}{m_{\rm D}}-\frac{1}{m_{\rm H}}\right)\Delta V^{\rm Ad}(r_1,r_2,\theta), \tag{17}$$

and

$$\Delta V^{\rm D_2O}(r_1,r_2,\theta)=\left(\frac{1}{m_{\rm D}}-\frac{1}{m_{\rm H}}\right)[\Delta V^{\rm Ad}(r_1,r_2,\theta)+\Delta V^{\rm Ad}(r_2,r_1,\theta)]. \tag{18}$$

TABLE IX. Low-lying vibrational levels for various isotopic substitution (in cm^{-1}).

Source	$H_2{}^{17}O$	$H_2{}^{18}O$	$HD^{16}O$	$D_2{}^{16}O$	$D_2{}^{18}O$	$T_2{}^{16}O$	$HT^{16}O$
				010			
V^{emp}	1591.36	1588.31	1403.42	1178.23	1170.01	995.18	1332.40
V^{mass}			1403.52	1178.41	1170.20	995.33	1332.49
V^{ZPST}	1591.36	1588.31	1403.52	1178.42	1170.18	995.39	1332.52
Expt.	1591.33[a]	1588.28[a]	1403.48[a]	1178.38[b]	1170.16[b]	995.33[c]	1332.48[d]
				020			
V^{emp}	3144.98	3139.05	2781.75	2336.48	2320.36	1976.25	2639.57
V^{mass}			2782.02	2336.84	2320.74	1976.57	2639.79
V^{ZPST}	3144.98	3139.05	2781.95	2336.85	2320.70	1976.66	2639.82
Expt.	3144.98[a]	3139.05[a]	2782.01[a]	2336.84[e]			
				100			
V^{emp}	3653.12	3649.67	2723.44	2671.33	2660.49	2236.79	2299.46
V^{mass}			2723.66	2671.65	2660.79	2237.26	2299.81
V^{ZPST}	3653.13	3649.66	2723.53	2671.41	2660.53	2236.88	2299.56
Expt.	3653.14[a]	3649.68[a]	2723.68[a]	2671.65[e]		2237.15[f]	2299.77[g]
				001			
V^{emp}	3748.35	3741.60	3707.58	2787.59	2767.37	2366.46	3716.79
V^{mass}			3707.48	2787.73	2767.51	2366.61	3716.72
V^{ZPST}	3748.33	3741.59	3707.50	2787.57	2767.31	2366.44	3716.72
Expt.	3748.32[a]	3741.57[a]	3707.47[a]	2787.72[e]		2366.60[h]	3716.58[f]

[a]HITRAN 96 database.
[b]Reference 59.
[c]Reference 55.
[d]Reference 58.
[e]Reference 54.
[f]Reference 53.
[g]Reference 56.
[h]Reference 57.

We represented ΔV^{Ad} using Eq. (4) with $i+j+k \leqslant 2$, which resulted in nine parameters. These parameters were optimized by simultaneously fitting the $HD^{16}O$ and $D_2{}^{16}O$ data. The final rms error for the combined $HD^{16}O$, $D_2{}^{16}O$ fit was 0.019 cm^{-1}, and the rms error for $HD^{16}O$ was 0.021 cm^{-1} and 0.017 cm^{-1} for $D_2{}^{16}O$. The results using this potential for these species are given in Table IX in the row labeled V^{mass}, and the agreement with experiment is much improved, with maximum error of only 0.04 cm^{-1}. The parameters for this correction are available from E-PAPS.[32] We initially tried to parameterize ΔV^{Ad} just using $HD^{16}O$ lines, but the correction we obtained did not perform very well for the other hydrogen isotopes. For that fit, the rms error of 0.019 cm^{-1} was only marginally better than what we obtained when fitting both $HD^{16}O$ and $D_2{}^{16}O$. This suggests that we were using more parameters than warranted by the available data.

We have used the PES V^{mass} to predict all of the $HD^{16}O$ lines in the HITRAN 96 database, and the band-by-band results are given in Table XII. Of the 9226 lines in the database, we are able to match 9221. The five unmatched lines are weak and appear to be missassigned, because the initial and final parities are the same, and so violate dipole selection rules. The results are very good for all bands, and as before we see a number of outliers: we estimate that 1.9% of the lines are incorrect. Over all bands, the 5, 10, 25, 50, 75, 90, and 95 percentile differences between the calculated and observed line positions are -0.04, -0.03, -0.02, 0.00,

TABLE X. Comparison between HITRAN 96 and results from V^{emp} by vibrational bands for $H_2{}^{17}O$. Frequencies are in cm^{-1} and intensity in cm/molecule.

			Line positions				Intensities[a]		
			Error percentiles						
Band	No. Lines	No. Outliers	25%	50%	75%	Max. abs. error	Summed HITRAN	Summed ratio	Max. ratio
000 000	622	12	0.00	0.00	0.01	0.30	1.94(−20)[b]	1.04	1.2
010 010	117	5	0.00	0.00	0.00	0.04	7.84(−24)	1.04	1.1
010 000	872	23	0.01	0.02	0.03	0.59	3.98(−21)	1.09	1.5
020 010	210	2	−0.04	−0.04	−0.03	0.06	3.54(−24)	1.01	1.3
020 000	247	3	−0.02	−0.01	0.00	0.06	2.40(−23)	1.30	1.8
100 000	387	5	−0.03	−0.02	−0.02	0.06	1.70(−22)	1.33	59.
001 000	529	16	0.02	0.03	0.04	0.14	2.52(−21)	1.25	1.4
111 000	226	5	−0.72	−0.64	−0.57	20.75	1.77(−23)	0.98	2.1
201 000	173	10	−0.78	−0.74	−0.67	2.00	7.33(−24)	0.79	2.7

[a]The theoretical intensities are multiplied by the isotope abundance factor 3.799×10^{-4}.
[b]$1.94(-20) = 1.94 \times 10^{-20}$.

TABLE XI. Comparison between HITRAN 96 and results from V^{emp} by vibrational bands for $H_2{}^{18}O$. Frequencies are in cm^{-1} and intensity in cm/molecule.

			Line positions				Intensities[a]		
			Error percentiles						
Band	No. Lines	No. Outliers	25%	50%	75%	Max. abs. error	Summed HITRAN	Summed ratio	Max. ratio
000 000	766	25	0.00	0.00	0.01	0.14	1.07(−19)[b]	0.99	1.3
010 010	202	9	0.00	0.00	0.00	0.14	4.61(−23)	0.99	1.1
010 000	968	34	0.01	0.02	0.03	9.36	2.15(−20)	1.06	2.7
020 010	262	3	−0.04	−0.03	−0.03	0.06	1.98(−23)	0.97	2.5
020 000	388	12	−0.01	−0.01	0.00	1.19	1.32(−22)	1.26	1.8
100 000	553	3	−0.03	−0.02	−0.01	0.10	9.47(−22)	1.27	220
001 000	711	24	0.02	0.03	0.04	0.39	1.39(−20)	1.18	1.3
011 010	101	3	−0.07	−0.06	−0.06	0.07	5.19(−24)	1.29	1.4
110 000	443	16	0.03	0.05	0.07	6.16	5.64(−23)	1.23	3.0
011 000	734	39	−0.04	−0.04	−0.03	9.58	1.48(−21)	1.23	3.1
031 000	102	3	−3.75	−3.65	−3.43	17.41	1.59(−24)	0.27	26
111 000	335	7	0.19	0.34	0.45	22.04	9.66(−23)	0.95	5.9
012 000	152	4	−3.05	−2.96	−2.79	17.07	2.80(−24)	0.57	9.0
121 000	140	3	0.43	0.50	0.61	20.60	3.80(−24)	1.71	2.9
201 000	279	21	0.08	0.18	0.34	5.03	4.06(−23)	0.75	3200
003 000	147	6	−6.10	−5.97	−5.71	13.37	4.48(−24)	0.90	1.7

[a]The theoretical intensities are multiplied by the isotope abundance factor 1.997×10^{-3}.
[b]$1.07(-19)=1.07\times10^{-19}$.

0.01, 0.03, and 0.04 cm^{-1}. The ratios of the summed intensities are in very good agreement, except for the last two bands, where the ratio is close to three.

Returning again to Table IX, we give our predictions for three other isotopically substituted water molecules. Comparing the use of V^{emp} and V^{mass} with experimental results, we see that V^{mass} greatly improves the results for all cases except ν_3 for HTO, where V^{mass} is only a slight improvement. The largest errors remaining are for ν_1 of T_2O (0.11 cm^{-1}) and ν_3 of HTO (0.14 cm^{-1}). The experimental data for these fundamentals is rather old,[53] and may be subject to larger errors. However, for both these molecules, the other stretching frequency is also given, and it agrees well with the more modern results quoted in Table IX, so the discrepancies may be real.

Recently Zobov *et al.*[37] have computed the diagonal adiabatic correction for water using *ab initio* wave functions. They find that the correction due to oxygen motion is very small, which is what we observed. We have added the difference between their correction for a given isotopically substituted species and their correction for $H_2{}^{16}O$ to V^{emp}, and computed the frequencies that are labeled V^{ZPST} in Table IX. We see that the results obtained using this adiabatic correction sometimes agree well with V^{mass}, sometimes going in the correct direction but not far enough, and sometimes going in the wrong direction. It is not clear if this is due to the approximate electronic wave functions used in Ref.(37) or to the neglect of other factors, such as mass polarization, which are included when we empirically determine the correction.

TABLE XII. Comparison between HITRAN 96 and results from V^{mass} by vibrational bands for $HD^{16}O$. Frequencies are in cm^{-1} and intensity in cm/molecule.

			Line positions				Intensities[a]		
			Error percentiles						
Band	No. Lines	No. Outliers	25%	50%	75%	Max. abs. error	Summed HITRAN	Summed ratio	Max. ratio
000 000	1382	44	−0.02	0.00	0.00	1.54	1.17(−20)[b]	1.02	6.1(+1)
010 000	1653	11	0.01	0.02	0.03	0.27	2.82(−21)	1.05	1.3(+2)
001 000	1333	31	−0.03	−0.02	0.00	0.29	6.33(−22)	1.04	3.1(+4)
020 000	953	25	−0.02	−0.01	0.00	0.35	8.42(−23)	1.02	2.8(+3)
100 000	1646	39	−0.01	0.01	0.02	7.59	1.42(−21)	1.05	1.6(+1)
011 000	860	5	−0.02	−0.01	0.01	4.59	6.42(−23)	1.01	9.4(+1)
030 000	602	8	−0.04	−0.02	−0.01	14.87	3.50(−23)	1.00	7.0(+1)
110 000	576	9	−0.02	−0.01	0.00	0.64	3.66(−23)	3.03	6.7(+0)
002 000	216	3	−0.04	−0.02	0.00	35.96	1.58(−23)	2.69	3.3(+0)

[a]The theoretical intensities are multiplied by the isotope abundance factor 2.992×10^{-4}.
[b]$1.07(-20)=1.07\times10^{-20}$.

TABLE XIII. Differences between various PESs and $V^{5Z}+\Delta V^{core}+0.87\Delta V^{basis}$. Energies in cm^{-1}.

Range	No. points	V^{BO}	V^{emp}	PJT	PJT2	W
0–500	36	3.1[a]	3.9	1.9	4.6	5.9
		8.7[b]	8.0	4.0	9.4	12.4
500–1000	16	6.4	8.5	3.2	7.8	12.6
		10.8	12.9	7.8	15.1	17.3
1000–5000	47	14.0	13.6	12.0	14.6	18.8
		30.8	27.5	40.5	37.3	38.6
5000–10 000	47	25.5	24.7	60.4	62.6	31.3
		56.8	46.8	191.6	179.7	55.2
10 000–15 000	60	32.6	29.4	125.1	133.1	57.8
		77.7	58.7	385.6	428.8	166.8
15 000–20 000	45	44.3	40.2	290.4	309.0	111.7
		90.2	64.8	675.8	722.6	464.4
20 000–25 000	55	46.3	44.2	622.6	618.0	386.4
		116.5	80.3	1823.6	1868.9	1261.1
25 000–30 000	49	50.0	42.8	1263.5	1358.1	906.6
		119.3	84.1	3656.5	3690.1	3010.3

[a]First row is root mean square error.
[b]Second row is maximum error.

IX. COMPARING THE *AB INITIO* RESULTS AND EMPIRICAL PES

We have seen that it is possible to modify the *ab initio* PES and reduce the errors in the line positions by two orders of magnitude. The next issue is how much of a change in the PES was required and whether the change is consistent with the expected errors of the *ab initio* results. Another issue of interest is the difference between the fully empirical PES[9–11] and the present PES.

In Table XIII we compare the potentials V^{BO}, V^{emp}, PJT,[9] PJT2,[10] and W (Refs. 11 and 60) with the *ab initio* data. We do not consider the PES of Ref. 61, for those workers apparently did not converge their vibrational wave functions sufficiently well to obtain meaningful results. In Table XIII we give statistics on the difference between a particular PES and our best estimate of the Born–Oppenheimer PES, namely $V^{5Z}+\Delta V^{core}+0.87\Delta V^{basis}$. The points selected are those used to generate V^{5Z}. First consider V^{BO} and V^{emp}. Below 5000 cm^{-1}, V^{BO} and V^{emp} give comparable differences. Above 10 000 cm^{-1}, V^{BO} gradually gets worse. Presumably the reason for this is that the adiabatic correction, which was determined using only low-lying energy levels, becomes less accurate and overestimates the effect as the energies increase. Now consider the three fully empirical PES. Below 5000 cm^{-1}, PJT is the best, while for higher energies W is better. It is often significantly better. The comparison given in Table XIII makes no real distinction between the PJT and PJT2 potentials. Now compare the fully empirical PES to V^{emp}. Below 1000 cm^{-1}, PJT does better than V^{emp}, but is probably not significantly different given the uncertainties in the *ab initio* calculations. Below 10 000 cm^{-1}, W and V^{emp} are close. At higher energies, V^{emp} is in significantly better agreement with the *ab initio* data than the fully empirical potentials.

It should be noted that all three fully empirical potentials are very similar in that they use the Jensen[33] functional form. The PJT2 PES also includes the Choi and Light[36] correction for small HH distances. The number of unique linear parameters for each potential is 26 for PJT, 27 for PJT2, and 47 for W. Thus, it appears likely that the PJT and PJT2 potentials require more terms to approach the true PES, and when more terms are added, the results will get closer to V^{emp}. However, a fully empirical PES will probably never get the very high portions of the PES correct. It is also interesting to note that the maximum differences in the surfaces are significantly larger than the differences in the computed transition frequencies. This suggests that the uniqueness of an empirical potential would require information about the true functional form of the potential, otherwise the potential can only hope to do well for regions of the PES that have the greatest influence on the fitted energy levels.

We can compare V^{emp} to our most reliable *ab initio* data, which is given in Table III. Adding the core correction to the extrapolated energies yields a maximum difference of 30 cm^{-1}, which occurs at 170°, which is a great improvement over the 151 cm^{-1} error produced by just using the 5Z PES. In all cases, V^{emp} is in closer agreement with our best estimate than the 5Z energy. The rms difference drops from 94 to 17 cm^{-1} from going from 5Z, which was the starting point in our optimization, to V^{emp}. Thus, the changes made to the *ab initio* data are consistent with the expected errors in the calculations.

In Table XIV we give the equilibrium geometries, harmonic, and fundamental frequencies for the potentials generated in the present work as well as the empirical PJT, PJT2, and W potentials. The results used the PES from the present work and W PES use nuclear masses, while the PJT and PJT2 PESs both use atomic masses. Changing to the nuclear mass raises the stretching levels by about 1 cm^{-1} and the bending level by about 0.4 cm^{-1}. By construction, V^{emp}, PJT, PJT2, and W agree very well with the fundamentals, but PJT and PJT2 have fairly large differences in other quantities, as compared to V^{emp} and W. For example, the harmonic asymmetric stretch frequency differs by 4 cm^{-1} between V^{emp} and PJT2.

In Table XV we give the quartic derivatives of the potentials determined in the present work evaluated at their respective equilibrium geometries. The differences among the potentials are not that great. This again shows that the empirical modifications to the PES needed to improve the agreement with the experimental data are small.

X. CONCLUSIONS

We have presented a new PES and DMS for H_2O obtained from high-quality *ab initio* electronic structure calculations at a large number of geometries. The PES was then empirically modified to match experimental line positions for $H_2{}^{16}O$. The empirical PES was called V^{emp}. Having accurate fits to the *ab initio* data and separately including core correlation were critically important to obtain the level of agreement with the experiment that is reported here; 66% of the experimental lines are matched with errors of less than 0.05 cm^{-1}. It appears that about 3% in the lines in the HITRAN 96

TABLE XIV. Equilibrium geometries, harmonic frequencies, and fundamental frequencies for $H_2{}^{16}O$ using various potentials.

	V^{5Z}	$V^{5Z}+\Delta V^{core}$	V^{BO}	V^{emp}	PJT[a]	PJT2[b]	W[c]
r_e(Å)	0.958 65	0.957 69	0.957 71	0.957 84	0.957 63	0.957 92	0.958
θ_e	104.348	104.481	104.479	104.508	104.510	104.500	104.493
ω_{ss}(cm^{-1})	3830.70	3838.14	3834.62	3833.79	3830.83	3830.38	3833.44
ω_b(cm^{-1})	1653.10	1652.42	1650.16	1649.50	1650.16	1649.59	1649.03
ω_{as}(cm^{-1})	3940.48	3948.34	3945.78	3945.36	3942.13	3940.96	3945.13
ν_{ss}(cm^{-1})	3653.73	3660.99	3657.56	3657.04	3657.09	3657.13	3656.88
ν_b(cm^{-1})	1598.40	1597.60	1595.36	1594.78	1594.68	1594.66	1594.54
ν_{as}(cm^{-1})	3750.93	3758.64	3756.36	3755.95	3755.84	3755.83	3755.77
zpe(cm^{-1})	4636.16	4642.92	4639.27	4638.39	4636.87	4634.76	4637.97

[a]PES from Ref. 9, using atomic masses.
[b]PES from Ref. 10, using atomic masses.
[c]PES from Ref. 11, using nuclear masses.

database are either wrong or missassigned. V^{emp} extrapolates to high J well in spite of the fact that in the optimization only low J ($\leqslant 5$) were used.

V^{emp} is decomposed into a mass-independent part and a mass-dependent correction, which is determined by fitting simultaneously data for $HD^{16}O$ and $D_2{}^{16}O$. This mass dependent correction also gives good results for $T_2{}^{16}O$ and $HT^{16}O$. No mass correction appears to be required for the different oxygen isotopes.

No nonadiabatic effects are explicitly included in the present work. The small errors obtained in the present work probably indicate that nonadiabatic effects are small. The present calculations use the nuclear rather than the atomic mass in the rovibrational calculations. It is shown that for low-lying levels, to within 0.02 cm^{-1} changing from one mass to the other is equivalent to scaling the coordinates in the potential. Thus, if nonadiabatic effects can be accounted for by changing to the atomic masses, they are on the order of 0.02 cm^{-1}.

There are some signs that the present PES is not perfect. The core correlation correction is scaled by 1.635 while calibration calculations indicate that the correct scaling factor should be less than one, the level of agreement without explicitly including nonadiabatic effects is perhaps a bit too good, and the errors do increase with J, although that issue is clouded by apparent errors in the experimental database. Just because we fit a substantial fraction of the experimental data well does not guarantee that the PES is correct. Thus, further work, both experimental and theoretical, on this problem is warranted.

The mass-dependent PES described in this work has been used to generate a high-temperature opacity database for $H_2{}^{16}O$, $H_2{}^{18}O$, $H_2{}^{17}O$, and $HD^{16}O$. This data is available from the authors upon request.[48]

ACKNOWLEDGMENTS

This work is partially supported by the Ames Director's Discretionary Fund and the NASA Astrophysics Theory Pro-

TABLE XV. Derivatives of various potentials evaluated at their equilibrium geometries. Energy in mdyne and bond lengths in Å.

r_1	r_2	θ	V^{5Z}	$V^{5Z}+\Delta V^{core}$	V^{emp}
0	0	2	7.070 686 3(−1)[a]	7.049 310 7(−1)	7.026 577 7(−1)
0	0	3	−7.064 267 3(−1)	−7.086 985 3(−1)	−7.049 966 3(−1)
0	0	4	−7.673 332 4(−1)	−7.656 649 0(−1)	−7.584 447 0(−1)
0	1	1	2.590 477 3(−1)	2.588 432 8(−1)	2.582 489 8(−1)
0	1	2	−3.165 163 1(−1)	−3.148 878 6(−1)	−3.183 616 0(−1)
0	1	3	7.190 163 9(−1)	7.176 189 9(−1)	7.201 990 3(−1)
0	2	0	8.442 539 7(+0)	8.475 828 5(+0)	8.459 850 0(+0)
0	2	1	−1.062 230 0(−1)	−1.014 980 7(−1)	−1.068 399 1(−1)
0	2	2	−3.549 439 1(−1)	−3.457 226 2(−1)	−3.177 874 2(−1)
0	3	0	−5.863 753 4(+1)	−5.890 500 5(+1)	−5.876 051 2(+1)
0	3	1	−1.501 760 1(+0)	−1.502 595 0(+0)	−1.497 812 9(+0)
0	4	0	3.642 467 2(+2)	3.661 714 4(+2)	3.654 764 5(+2)
1	1	0	−1.009 889 1(−1)	−1.006 775 3(−1)	−1.034 810 6(−1)
1	1	1	−5.169 086 1(−1)	−5.143 763 1(−1)	−5.156 029 7(−1)
1	1	2	6.745 484 6(−1)	6.786 138 2(−1)	6.859 168 5(−1)
1	2	0	−7.179 685 2(−2)	−7.222 075 6(−2)	−6.934 259 2(−2)
1	2	1	3.239 628 9(−1)	3.217 049 4(−1)	3.541 147 4(−1)
1	3	0	−6.858 435 8(−1)	−7.097 695 3(−1)	−6.665 494 0(−1)
2	2	0	5.155 454 7(−1)	4.972 972 9(−1)	4.416 614 4(−1)

[a]7.0706863(−1)=7.0706863×10^{-1}.

gram. The authors would also like to thank Duane Carbon for his support and encouragement of this work and Richard Wattson for useful discussions, and for giving us a copy of his PES parameters, Richard Freedman for supplying us with a copy of the HITRAN database, Nick Handy for comments on the manuscript, and Jonathan Tennyson for comments on the manuscript and supplying us with a copy of the PJT2 PES prior to publication. The *ab initio* calculations were carried out using a grant of computer time from the Numerical Aeronautics Simulation Facility at the NASA Ames Research Center.

APPENDIX

The differences from the algorithm of Ref. 39 are as follows. We now use analytic basis functions to describe the stretching degrees of freedom. For the hyperradius ρ, which transforms as the symmetric stretch, the SCF equation takes the form[39]

$$-\frac{\hbar^2}{2\mu}\frac{d^2}{d\rho^2}\psi_n(\rho)+V^{\mathrm{SCF}}(\rho)\psi_n(\rho)=E_n\psi_n(\rho), \tag{A1}$$

with ρ having the domain $[0,\infty]$. We will expand ψ_n in terms of the primitive basis

$$\phi_n(\rho)=N_n x^{\alpha/2}\exp(-x/2)L_n^{(\alpha)}(x), \tag{A2}$$

with $x=\xi\rho$, ξ and α parameters, N_n a normalization constant, and $L_n^{(\alpha)}$ a generalized Laguerre polynomial.[62] These polynomials are orthogonal with respect to the weight function $x^{\alpha}\exp(-x)$ on the interval $[0,\infty]$. In the absence of round-off error, the kinetic energy matrix elements are given exactly by quadrature:

$$T_{nn'}=\frac{2\hbar^2}{\mu}N_nN_{n'}\sum_{i=1}^{N} w_i[L_n^{(\alpha)}(x_i)(\alpha-x_i)+2x_iL_n^{(\alpha)\prime}(x_i)] \times[L_{n'}^{(\alpha)}(x_i)(\alpha-x_i)+2x_iL_{n'}^{(\alpha)\prime}(x_i)], \tag{A3}$$

where w_i and x_i are the Gaussian quadrature weights and nodes for the weight function $x^{\alpha-2}\exp(-x)$ and $N>\max(n,n')+2$. The potential matrix elements are also evaluated by Gaussian quadrature. The quadrature weights and nodes can be computed using, e.g., the routines from Ref. 49. The $L_n^{(\alpha)}$ and $L_n^{(\alpha)\prime}$ can be easily computed from recursion relations.

The final ingredients in our basis are the parameters α and ζ. We determine them by matching the position and relative curvature of ϕ_0 to the harmonic wave function. This results in the relations

$$\zeta=2\rho_e\mu\omega/\hbar, \tag{A4}$$

and

$$\alpha=\zeta\rho_e, \tag{A5}$$

with ω the harmonic frequency and ρ_e the equilibrium bond length. For H_2O, on the first SCF iteration for $JPS=0++$ (at this point in the iterations the bending angle is fixed at its equilibrium value and the PES is averaged over the lowest function for the hyperangle), we have $\zeta=161/a_o$ and $\alpha=403$. Because α is large, it is advantageous to write

$$N_n=\left[\frac{\Gamma(n+1)\zeta}{\Gamma(\alpha+n+1)}\right]^{1/2} =\left[\frac{\Gamma(\alpha+1)\Gamma(n+1)}{\Gamma(\alpha+n+1)}\right]^{1/2}\left[\frac{\zeta}{\Gamma(\alpha+1)}\right]^{1/2}, \tag{A6}$$

and include the first factor in the polynomials and the square of the second factor in the quadrature weights. To deal with the large numbers produced by using large α, one can use logarithms for intermediate quantities and then exponentiate the result.

These basis functions are reasonably efficient—using a single function gives an energy within 92 cm^{-1} of the converged result for the ground vibrational level. Also the results are very stable when using large numbers of basis functions. It should be noted that all inverse powers of ρ up to α give rise to finite matrix elements and can be evaluated exactly by quadrature. This basis is similar to that introduced by Kauppi,[63] except that $x=\xi/\rho$ and $\alpha=1/2$ were used.

When determining the optimized quadrature weights and nodes[64] for the contracted functions, we made two changes. First, the weight function was taken to be the sum of the squares of all the contracted ρ functions, divided by ρ^2. Second, rather than using matrix elements of powers of $\rho-\rho_e$ to generate the quadrature nodes, we used matrix elements of powers of $\rho-\rho_o$, with ρ_o an adjustable parameter. We then varied ρ_o to minimize the root-mean-square size of the matrix elements of the powers. These changes were necessary to give numerical stability to the determination of the quadrature nodes when large numbers of points were desired for a large number of contracted functions.

For the hyperangle χ, which transforms like the asymmetric stretch, the SCF equation takes the form[39]

$$-\frac{\hbar^2}{2\mu}\frac{d^2}{d\chi^2}\psi_n(\chi)+V^{\mathrm{SCF}}(\chi)\psi_n(\chi)=E_n\psi_n(\chi), \tag{A7}$$

with χ having the domain $[0,\pi/2]$. Coupling terms in the full kinetic energy require the evaluation of the operators $\sin^{-2}\chi$ and $\cos^{-2}\chi$, which gives rise to singularities at 0 and $\pi/2$.

In this case, we make the transformation

$$x=\cos 2\chi, \tag{A8}$$

and use as primitive basis functions

$$\phi_n(\chi)=N_n(1-x)^{\alpha/2+1/4}(1+x)^{\beta/2+1/4}P_n^{(\alpha,\beta)}(x), \tag{A9}$$

where N_n is a normalization constant, α and β are parameters, and $P_n^{(\alpha,\beta)}$ is a Jacobi polynomial.[62] These polynomials are orthogonal with respect to the weight function $(1-x)^{\alpha}(1+x)^{\beta}$ on $[-1,1]$. The extra factors of 1/4 in Eq. (A9) come from the Jacobian determinant. Then, in the absence of round-off error, the kinetic energy matrix elements can be computed exactly by quadrature, i.e.,

$$T_{nn'}=\frac{\hbar^2}{2\mu}N_nN_{n'}\sum_{i=1}^{N} w_iD_n^{(\alpha,\beta)}(x_i)D_{n'}^{(\alpha,\beta)}(x_i), \tag{A10}$$

where

$$D_n^{(\alpha,\beta)}(x)=P_n^{(\alpha,\beta)}(x)[(\alpha+\tfrac{1}{2})(1+x)-(\beta+\tfrac{1}{2})(1-x)] -2(1-x^2)P_n^{(\alpha,\beta)\prime}(x), \quad \text{(A11)}$$

w_i and x_i are the Gaussian quadrature weights and nodes for the weight function $(1-x)^{\alpha-1}(1+x)^{\beta-1}$ and $N>\max(n,n')+2$. If

$$V^{\mathrm{SCF}}(\chi)=(1+x)^{-\delta}(1-x)^{-\gamma}\sum_{i=0}^{p} v_i x^i, \quad \text{(A12)}$$

then provided $\delta<\beta$ and $\gamma<\alpha$, the potential matrix elements will be given exactly by the Gaussian quadrature from the weight function $(1-x)^{\alpha-\gamma}(1+x)^{\beta-\delta}$. Since $2\cos^2\chi=1+x$ and $2\sin^2\chi=1-x$, the singular operators in the kinetic energy coupling can also be evaluated exactly when $\alpha,\beta>1$.

To determine α and β, we proceed as before and match ϕ_0 to the harmonic oscillator wave function. This produces

$$\beta=(1+\cos 2\chi_e)\mu\omega/4-\tfrac{1}{2}, \quad \text{(A13)}$$

and

$$\alpha=[\beta(1-\cos 2\chi_e)-\cos 2\chi_e]/(1+\cos 2\chi_e), \quad \text{(A14)}$$

where χ_e is the equilibrium value of χ. On the first SCF iteration, (at this point the other coordinates are fixed at their equilibrium values), we have $\alpha=\beta=51$, and approximating ψ_0 by ϕ_0 yields an energy within 1.5 cm^{-1} of the converged result. Thus, this is a very efficient basis set.

One could also use a linear transformation of χ instead of Eq. (A8) to give a function having the domain $[-1,1]$. However in that case, matrix elements of $\sin^{-2}\chi$ and $\cos^{-2}\chi$ would not be given exactly by quadrature.

When computing the optimized quadrature nodes, the weight function is taken to be the sum of the square of all the contracted χ functions, divided by $\cos^2\chi\sin^2\chi$ and powers of x were used to generate the quadrature. Thus, all functions of the form of Eq. (A12) with $\delta=\gamma=1$ and $p\leqslant n_\chi-1$, with n_χ the total number of quadrature points (i.e., 14 for $JPS=0++$), will be integrated exactly.

Since the body frame z axis was aligned along one of the Radau vectors, the primitive rotation–bending functions are not symmetric with respect to exchanging the two H atoms. However, the converged functions obtained by diagonalizing the rotation–bending part of the Hamiltonian either have the full symmetry, or are linear combinations of degenerate functions that have the full symmetry. This diagonalization is part of the SCF procedure. To determine the symmetry and to unmix the degenerate levels, we proceeded as follows: We evaluated the functions and the permutation operator acting on the functions at 100 randomly chosen configurations, and then we applied the techniques described in Ref. 39 to produce functions of pure symmetry. This is an inexpensive step. Only those functions whose root-mean-square deviation from the average of the symmetry eigenvalue was less than 0.01 were deemed pure enough to use in subsequent steps of the calculation. This reduced the effective value of the energy cutoff parameter for high J.

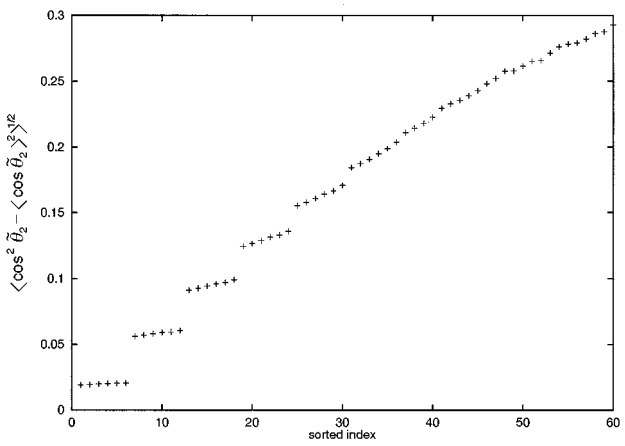

FIG. 9. Sorted $\langle\cos^2\tilde{\theta}_2-\langle\cos\tilde{\theta}_2\rangle^2\rangle^{1/2}$ for rotation-bending functions for $JPS=10++$.

In the present work, we performed the diagonalization in two steps: first we coupled all functions with a given Ω, and then we coupled only those functions with energies below a cutoff energy. In the present application, the first diagonalization step is not really necessary since Ω is not even remotely a good quantum number and essentially all functions from each Ω were used.

To assign approximate rotation–bending quantum numbers, the expectation value of the deviation of $\cos\tilde{\theta}_2$ from its average value was computed and then sorted into ascending order. An example of this is given in Fig. 9 for $JPS=10++$. Figure 9 shows a stair step structure, and the first step is for $\nu_2=0$, the second for $\nu_2=1$, etc. For low ν_2 and low to moderate J, there is very little mixing between bend and rotation, so clear steps appear. For higher ν_2 and high J, there is more mixing and the step structure disappears. Nonetheless, we use a procedure based on this for all J and ν_2. Specifically, after the sort, the first n_{rot}^{JPS} functions are assigned a bending quantum number of zero, etc, where n_{rot}^{JPS} is the number of rigid rotator functions of the particular JPS of interest. Then for each ν_2, the rotational levels were labeled by the rigid rotator quantum numbers, and the particular choices were made by ordering both by energy.

To assign approximate quantum numbers for the rovibrational levels, we simply determined the eigenvector component of largest magnitude. Then the symmetric stretch quantum number was the number of nodes in the hyperradius basis function of this component, the asymmetric stretching quantum number was the number of nodes in the hyperangle basis function of this component, and the rotation–bending quantum numbers were taken from the assigned values of the rotation–bending function of this component.

[1] L. Wallace, P. Bernath, W. Livingston, K. Hinkle, J. Busler, B. Guo, and K. Zhang, Science **268**, 1155 (1995).
[2] T. Tsuji, Annu. Rev. Astron. Astrophys. **24**, 89 (1986).
[3] U. G. Jørgensen, in *Molecules in the Stellar Environment*, edited by U. G. Jørgensen (Springer-Verlag, Berlin, 1994), p 29.
[4] U. G. Jørgensen and P. Jensen, J. Mol. Spectrosc. **161**, 219 (1993).
[5] S. Miller, J. Tennyson, H. R. A. Jones, and A. J. Longmore, in *Molecules*

in the Stellar Environment, edited by U. G. Jørgensen (Springer-Verlag, Berlin, 1994), p 296.
[6] S. Viti, J. Tennyson, and O. L. Polyansky, Mon. Not. R. Astron. Soc. (submitted).
[7] C. W. Bauschlicher and S. R. Langhoff, Science **254**, 394 (1991).
[8] J. M. L. Martin and P. R. Taylor, Chem. Phys. Lett. **225**, 473 (1994).
[9] O. L. Polyansky, P. Jensen, and J. Tennyson, J. Phys. Chem. **101**, 7651 (1994).
[10] O. L. Polyansky, P. Jensen, and J. Tennyson, J. Phys. Chem. **105**, 6490 (1996).
[11] R. B. Wattson (personal communication).
[12] R. J. Bartlett, S. J. Cole, G. D. Purvis, W. C. Ermler, H. C. Hsieh, and I. Shavitt, J. Chem. Phys. **87**, 6579 (1987).
[13] W. H. Green, A. Willetts, D. Jayatilaka, and N. C. Handy, Chem. Phys. Lett. **169**, 127 (1990).
[14] J. M. L. Martin, J. P. François, and R. Gijbels, J. Chem. Phys. **95**, 8374 (1991).
[15] W. Gabriel, E. A. Reinsch, P. Rosmus, S. Carter, and N. C. Handy, J. Chem. Phys. **99**, 897 (1993).
[16] H. G. Kjaergaard, B. R. Henry, H. Wei, S. Lefebvre, T. Carrington, O. S. Mortensen, and M. L. Sage, J. Chem. Phys. **100**, 6228 (1994).
[17] L. S. Rothman, R. R. Gamache, R. H. Tipping, C. P. Rinsland, M. A. H. Smith, D. C. Benner, V. M. Devi, J.-M. Flaud, C. Camy-Peyret, A. Perrin, A. Goldman, S. T. Massie, L. R. Brown, and R. A. Toth, J. Quant. Spectrosc. Radiat. Transf. **48**, 469 (1992).
[18] L. S. Rothman, J. Schroeder, A. McCann, R. R. Gamache, R. B. Wattson, J.-M. Flaud, A. Perrin, V. Dana, J.-Y. Mandin, A. Goldman, S. Massie, P. Varanasi, and K. Yoshino, J. Quant. Spectrosc. Radiat. Transf. (to be published).
[19] T. H. Dunning, J. Chem. Phys. **90**, 1007 (1989); R. A. Kendall, T. H. Dunning, and R. J. Harrison, J. Chem. Phys. **96**, 6796 (1992); D. E. Woon, K. A. Peterson, and T. H. Dunning (unpublished).
[20] D. E. Woon, K. A. Peterson, and T. H. Dunning (unpublished); oxygen *h* and *i* functions from D. Feller.
[21] C. W. Bauschlicher and H. Partridge, J. Chem. Phys. **100**, 4329 (1994); H.-J. Werner and P. J. Knowles, Chem. Phys. Lett. **145**, 514 (1988).
[22] H.-J. Werner and P. J. Knowles, J. Chem. Phys. **89**, 5803 (1988).
[23] C. W. Bauschlicher, Theor. Chim. Acta (submitted).
[24] R. J. Gdanitz and R. Ahlrichs, Chem. Phys. Lett. **143**, 413 (1988)
[25] R. J. Bartlett, Annu. Rev. Phys. Chem. **32**, 359 (1981).
[26] K. Raghavachari, G. W. Trucks, J. A. Pople, and M. Head-Gordon, Chem. Phys. Lett. **157**, 479 (1989).
[27] A. D. Pradhan, H. Partridge, and C. W. Bauschlicher, J. Chem. Phys. **101**, 3857 (1994); H. Partridge and C. W. Bauschlicher, J. Chem. Phys. **103**, 10589 (1995).
[28] D. Feller, J. Chem. Phys. **96**, 6104 (1992);D. E. Woon, Chem. Phys. Lett. **204**, 29 (1993); and J. Chem. Phys. **100**, 2838 (1994).
[29] J. M. L. Martin, Chem. Phys. Lett. **259**, 669 (1996).
[30] MOLPRO 94 is a package of *ab initio* programs written by H.-J. Werner and P. J. Knowles, with contributions from J. Almlöf, R. D. Amos, M. J. O. Deegan, S. T. Elbert, C. Hampel, W. Meyer, K. Peterson, R. Pitzer, A. J. Stone, and P. R. Taylor.
[31] MOLECULE-SWEDEN is an electronic structure program system written by J. Almlöf, C. W. Bauschlicher, M. R. A. Blomberg, D. P. Chong, A. Heiberg, S. R. Langhoff, P.-Å. Malmqvist, A. P. Rendell, B. O. Roos, P. E. M. Siegbahn, and P. R. Taylor.
[32] See AIP document No. E-PAPS: E-JCPSA-106-4618 for three ASCII files: the *ab initio* points, a FORTRAN subroutine to evaluate the PES, and a FORTRAN subroutine to evaluate the DMS. E-PAPS document files may be retrieved free of charge from our FTP server (http://www.aip.org/epaps/epaps.html). For further information: e-mail: paps@aip.org or fax: 516-576-2223.
[33] P. Jensen, J. Mol. Spectrosc. **128**, 478 (1988).
[34] J. N. Murrell, S. Carter, S. C. Farantos, P. Huxley, and A. J. C. Varandas, *Molecular Potential Energy Functions* (Wiley, Chichester, 1984).
[35] R. E. Howard, A. D. McLean, and W. A. Lester, J. Chem. Phys. **71**, 2412 (1979).
[36] S. E. Choi and J. C. Light, J. Chem. Phys. **97**, 7031 (1992).
[37] N. F. Zobov, O. L. Polyansky, C. R. Le Sueur, and J. Tennyson, Chem. Phys. Lett. **260**, 381 (1996). Note that $S_2=\cos\theta-\cos\theta_e$ and the units of $c_{i,j,k}$ are μE_h amu $a_o^{-(i+k)}$.
[38] J. R. Stallcop, H. Partridge, and E. Levin, Phys. Rev. A, **53**, 766 (1996).
[39] D. W. Schwenke, J. Phys. Chem. **100**, 2867 (1996); **100**, 18 884 (1996).
[40] D. W. Schwenke, Comput. Phys. Commun. **70**, 1 (1992).
[41] LAPACK, University of Tennessee, University of California Berkeley, NAG Ltd., Courant Institute, Argonne National Lab, and Rice University, March 31, 1993.
[42] S. Miller, J. Tennyson, and B. T. Sutcliffe, Mol. Phys. **66**, 429 (1989).
[43] G. Herzberg, *Molecular Spectra and Molecular Structure: III. Electronic Spectra and Electronic Structure of Polyatomic Molecules* (Van Nostrand Reinhold, New York, 1966).
[44] B. S. Garbow, K. E. Hillstrom, and J. J. More, Argonne National Laboratory, Minpack Project, March 1980.
[45] N. C. Handy and A. M. Lee, Chem. Phys. Lett. **252**, 425 (1996).
[46] P. R. Bunker and R. E. Moss, J. Mol. Spectrosc. **80**, 217 (1980).
[47] D. M. Bishop and S.-K. Shih, J. Chem. Phys. **64**, 162 (1986).
[48] The e-mail address of the authors are: partridg@pegasus.arc.nasa.gov and schwenke@pegasus.arc.nasa.gov
[49] W. H. Press, B. P. Flannery, S. A. Teukolsky, and W. T. Vetterling, *Numerical Recipes, Second edition* (Cambridge University Press, Cambridge, 1992).
[50] O. L. Polyansky, N. F. Zobov, J. Tennyson, J. A. Lotoski, and P. F. Bernath, J. Mol. Spectrosc. (submitted).
[51] O. L. Polyansky, J. R. Busler, B. Guo, K. Zhang, and P. F. Bernath, J. Mol. Spectrosc. **176**, 305 (1996).
[52] N. E. Klepeis, A. L. L. East, A. G. Császár, W. D. Allen, T. J. Lee, and D. W. Schwenke, J. Chem. Phys. **99**, 3865 (1993).
[53] G. Wilemski, J. Quant. Spectrosc. Radiat. Transf. **20**, 291 (1978).
[54] N. Papineau, J.-M. Flaud, C. Camy-Peyret, J. Mol. Spectrosc. **87**, 219 (1981).
[55] H. A. Fry, L. H. Jones, and J. E. Barefield, J. Mol. Spectrosc. **103**, 41 (1984).
[56] S. D. Cope, D. K. Russell, H. A. Fry, L. H. Jones, and J. E. Barefield, J. Mol. Spectrosc. **127**, 464 (1988).
[57] S. D. Cope, D. K. Russell, H. A. Fry, L. H. Jones, and J. E. Barefield, J. Mol. Spectrosc. **120**, 311 (1986).
[58] O. N. Ulenikov, V. N. Cherepanov, and A. B. Malikova, J. Mol. Spectrosc. **146**, 97 (1991).
[59] R. A. Toth, J. Mol. Spectrosc. **162**, 41 (1993).
[60] R. B. Wattson and L. S. Rothman, J. Quant. Spectrosc. Radiat. Transf. **48**, 763 (1992).
[61] D. Xie and G. Yan, Chem. Phys. Lett. **248**, 409 (1996).
[62] M. Abramowitz and I. A. Stegun, *Handbook of Mathematic Functions*, (Dover, New York, 1972).
[63] E. Kauppi, Chem. Phys. Lett. **229**, 661 (1994).
[64] D. W. Schwenke and D. G. Truhlar, Comput. Phys. Commun. **34**, 57 (1984).